SLAC – PUB – 3702
June 1985
(T/E)

Inclusive Production of Multi-Strange Hyperons from 11 GeV/c K^-p Interactions*

D. Aston[a], R.K. Carnegie[b], W. Dunwoodie[a], S. Durkin[a,1], P.G. Estabrooks[b], R. J. Hemingway[b], A. Honma[a,2], D. Hutchinson[a], W. B. Johnson[a], P.F.Kunz[a], T. Lasinski[a,3], D.W.G.S. Leith[a], L. Levinson[a,4], R. McKee[c,5], B. T. Meadows[d], A.C. McPherson[b], W.T. Meyer[a,6], G.K. Oakham[b,2], B.N. Ratcliff[a], S. Shapiro[a], T. Shimomura[a], S. Suzuki[a,7], J. Va'Vra[a], S. Williams[a].

ABSTRACT

Large samples of inclusively produced Ξ^-, Ω^- and $\Xi^\circ(1530)$ events are presented from a 1427 $ev/\mu b$ exposure of the LASS spectrometer to an 11 GeV/c K^- beam. Production characteristics of these states are compared with other data and shown to be consistent with hyperon exchange. Polarization of Ξ^- shows an increase in magnitude with both Feynman x and transverse momentum. The Ξ^- decay parameters are measured to be $\alpha_\Xi = -0.40 \pm 0.03$ and $\Phi_\Xi = (5 \pm 10)^\circ$. Results of searches for higher mass hyperons are presented. The $\Xi^-(1820) \to \Xi^\circ(1530)\pi^-$ decay is observed, while we fail to confirm the existence of the $\sum^+(3170)$.

Submitted to *Physical Review D*

---

* Work supported in part by the Department of Energy under contract No. DE-AC03-76SF00515, the National Research Council, Canada and the Natural Sciences and Engineering Research Council, Canada, and the National Science Foundation under grant No. PHY82-09144.

[a] Stanford Linear Accelerator Center, Stanford University, P.O.Box 4349, Stanford, California 94305, U.S.A.

[b] Carleton University, Ottawa, Ontario, Canada K1S 5B6.

[c] National Research Council, Ottawa, Ontario, Canada, K1A 0R6.

[d] University of Cincinnati, Cincinnati, Ohio 45221.

[1] Present address: University of Pennsylvania, Philadelphia, PA 19104, USA.

[2] Present address: CERN, CH-1211, Geneva 23, Switzerland.

[3] Present address: NASA, Ames Research Center, Mountain View, CA 94040, USA.

[4] Present address: Weizmann Institute of Science, Rehovot 76100, Israel.

[5] Present address: Los Alamos Scientific Laboratory, Los Alamos, NM 87545, USA.

[6] Present address: Iowa State University, Ames, IA 50011, USA.

[7] On leave from Nagoya University, Nagoya, Japan.

1. Introduction

Very little data on the inclusive production and decay characteristics of baryons with strangeness -2 or -3 have been reported in the literature. K^-p interactions have been studied at a variety of momenta from 4.2 to 16 GeV/c[1–7] to reveal Ξ^- inclusive characteristics, but detailed studies of Ξ° (1530) production data have been made only at 4.2 GeV/c;[1] at 8.25 GeV/c;[2] and, with very limited statistics, at 10 and 16 GeV/c.[3] The only study of Ω^- inclusive production has been at 8.25 GeV/c.[2] Each of these sets of data have come from bubble chamber experiments where the complex event topologies involved were readily recognized. Previous counter experiments have isolated large samples of Ξ^- and Ω^- particles, but have mainly concentrated in studying either an entirely different production mechanism from hyperon beam interactions with protons and deuterons,[8] or their weak decay modes,[9–13] and some discrepancies exist amongst these large experiments over the value of the $\Xi^- \to \Lambda\pi^-$ decay asymmetry parameter.

In this paper, we describe results from the first phase of an on-going study of data including the three hyperon production reactions:

K^-p	$\to \Xi^-$	+ anything	(12,550 events)	(1)
	$\to \Omega^-$	+ anything	(96 events)	(2)
	$\to \Xi^\circ(1530)$	+ anything	(1,110 events)	(3)

using the LASS spectrometer.[14] The raw exposure for the data presented here was 1427 ev/μb, and after including the effects of the average acceptances for these reactions—about 10% for Ξ^-, 5% for Ω^- and Ξ° (1530)—compares favorably with the largest of the bubble chamber experiments (with a reported exposure of 150ev/μb) in which samples of 8121 Ξ^-, 2772 Ξ° (1530), and 67 Ω^- were accumulated.[2]

The data presented here were accumulated by the LASS spectrometer equipped with spark chambers as vertex detectors and represent about 10% of the total

accumulation of such events. The remaining data, not reported here, were taken after a major upgrade in LASS to replace spark chambers by proportional wire chambers with a resolution approximately three times better. These latter data are presently being analyzed, and will be published later. Our experiment is outlined in Section 2. Reconstruction and isolation of clean samples of the above reactions was a difficult experimental procedure, which is described in detail in Section 3. The remaining sections present the results of the analysis. The cross sections are discussed in Section 4, our measurement of weak decay parameters for the Ξ^- in Section 5, and the results of a search for strange baryons in Section 6.

2. Description of the Experiment

The experiment was performed in an 11 GeV/c RF separated K^- beam directed at the LASS spectrometer[14] at SLAC. Details of the experiment have been given elsewhere,[15] and are only briefly reiterated here. Scintillation counter hodoscopes and 10 planes of proportional wire chambers with 1 *mm* wire spacing were located in the beam to measure the momentum and trajectory of the incident kaon.

The LASS spectrometer is shown schematically in Figure 1. It consists of a large superconducting solenoid vertex detector followed by a dipole spectrometer. The 23 *KGauss* solenoid field is parallel to the horizontal beam direction while the dipole field has a dominant vertical component with a field integral of 30 $KGauss - meters$ along the beam axis. Interaction products which have momenta $\lesssim$ 3 GeV/c and which are not produced too close to the beam axis are effectively measured by the solenoid while particles with momenta $\gtrsim$ 1.5 GeV/c close to the beam line are momentum analyzed in the dipole spectrometer.

The 91.6 *cm* long, liquid H_2 target was situated on the axis of the solenoid and was surrounded by an inner cylindrical proportional wire chamber (PWC) and five outer cylindrical capacitive-diode readout (CD) spark chambers arranged

coaxially, each having two spark gaps and providing three coordinate measurements. The region downstream of the target was instrumented with planar CD chambers, PWC planes and three segmented cathode readout foil chambers. The spark gaps were deadened in the high flux region around the solenoid axis because of their relatively long memory time. These deadened regions were overlapped by PWC's with 1 *mm* wire spacing and 26 by 26 *cm* active areas.

The dipole spectrometer, located downstream of the solenoid, consisted of a set of eight PWC planes, two CD spark chambers and two magnetostrictive readout (MS) spark chambers upstream from the dipole electromagnet; and four MS chambers, one PWC plane, and two segmented scintillator hodoscopes downstream of the dipole. Each MS chamber had two spark gaps and provided four coordinate measurements. Particle identification was provided by a large threshold-Čerenkov counter (C_1) which filled the downstream aperture of the solenoid; a 24-segment circular time-of-flight (TOF) array in the solenoid; and by a large, threshold-Čerenkov counter (C_2) downstream.

The very loose trigger, which essentially required two or more charged particles to emerge from the target, had almost complete acceptance for the events of interest here. An event was recorded if it had: 1) a well-measured incident kaon; 2) no particle remaining in the beam at the end of the spectrometer; 3) two or more hits outside a 3.2 *cm* square beam hole in the full aperture proportional chamber (T_1 in Figure 1) located 54 *cm* downstream of the target, and; 4) at least one TOF hit. Additional triggers were mixed with the event trigger to provide a sample of events to study the spectrometer performance.

3. Sample Selection

3.1 Preliminary Extraction

Isolation of our Ξ^- and Ω^- data samples is summarized in Tables I and II respectively, and described below. A total of 40 million triggers were recorded on tape. All events were processed through a preliminary analysis program whose major functions included track finding (grouping of the various coordinate readouts into tracks); track fitting (assigning momenta, etc); beam track reconstruction; and topology testing. Primary output from this program for each event then included a list of tracks with estimates of their momenta, and possible topological assignments relating tracks to production and decay vertices. The topology of interest to this study is illustrated in Figure 2. We also reconstructed events having an additional, visible K° decay. The p and π from the Λ decay were required to have an effective mass $1.10 \leq M_{p\pi^-} \leq 1.13$ GeV/c^2 at their point of closest approach and to point back to a negative track giving a $\Lambda\pi^-$ effective mass in the range 1.2 to 1.4 GeV/c^2 for a Ξ^- candidate, or a ΛK^- mass between 1.6 and 1.8 GeV/c^2 for an Ω^- candidate. The lengths of the reconstructed Λ, K° and Ξ^- (or Ω^-) connecting tracks were required to be at least 2 cms. The V^- candidate track is typically rather short and, indeed, Ξ^- and Ω^- particles have lifetimes such that they usually decay within the target volume. However, to reduce the large background from events with no real Ξ^- or Ω^-, the V^-connecting length was also required to be 2 *cms*. These loose criteria defined 405,000 preliminary candidates for the Ξ^- and Ω^- topologies which were extracted for further study.

After these requirements, the $\Lambda\pi^-$ effective mass distribution, shown in Figure 3, showed a clear Ξ^- signal. A fit to this mass plot[16] gave an estimated Ξ^- signal of 21,000 $\pm$ 250 above 30,000 background. However, because of the large remaining background, there was very little clearly observed Ω^- in the corresponding ΛK^- mass spectrum.

Table I

Selection Criteria for V^- Candidates

	Total Events Left	Signal/Background* in Ξ^- Range $1310 \leq M_{\Lambda\pi^-} \leq 1332$ MeV/c^2
Total triggers in experiment	40×10^6	
Primary Analysis indicates V^- topology is possible	405,000	21,002/29,773
Multi-vertex fit with confidence level $\gtrsim 10^{-6}$	184,960	17,942/13,786
$1.2 \leq M_{\Lambda\pi^-} \leq 1.4 GeV$ (Ξ^-) $1.6 \leq M_{\Lambda\pi^-} \leq 1.8 GeV$ (Ω^-)	109,940	17,942/13,786
Vertices correctly ordered after fitting	81,993	17,767/10,735
Vertices within fiducial volume	77,959	16,387/ 9,669
All tracks in time where determined	77,905	16,380/ 9,647
All tracks consistent with particle identification	67,997 55,200 (Ω)	15,859/ 7,825
Ξ^- (or Ω^-) production kinematically possible	65,213 52,852 (Ω)	15,573/ 7,292
Length of $V^- > 5cms$	22,841 2,304 (Ω)	12,553/ 963

* Estimated from fits to mass distributions.

Table II

Additional Ω^- Event Criteria

Requirement	Number Remaining	Signal/Background† $1.657 \leq M_{\Lambda K} \leq 1.687$
Length of $V^- > 5$ *cms* and $> 4\sigma$	2,304	—
Event is not Ξ^-	1,758	—
Confidence levels for both geometrical and Λ mass constrained fits $\gtrsim 2\%$	882	—
Cosine helicity > 0.475	579	125/115
$\Omega^- < 3.5$ decay lengths	501	96/80

† Estimated from fits to mass distributions.

3.2 GEOMETRIC CONSTRAINTS

The considerable backgrounds in these distributions resulted, primarily, from the fake V^-'s produced by combining Λ's with the large number of negative tracks available at the primary vertex. This problem was made more difficult because the spark chamber resolution was typically about 1 *mm*, and tracks near the vertices were often overlapped. In an attempt to improve the vertex resolution and hence to allow a cleaner V^- selection, all events from the samples described above were subjected to two multi-vertex fits, using all measured coordinates. The first constrained all tracks from a common vertex to emerge from a single point, and required the reconstructed Λ, K° or $\Xi^-(\Omega^-)$ tracks to have 3-momenta such as to correctly connect their beginning and ending vertices. In the second of these fits, the effective mass of the V° from the kink was constrained to be that of the Λ. Only events in which at least one of these fits was obtained with a confidence level greater than 10^{-6} and vertices correctly ordered and in acceptable fiducial volumes were considered further.

3.3 Particle Identification Cuts

Another major source of background arose from $\gamma \rightarrow e^+e^-$ or $K^\circ \rightarrow \pi^+\pi^-$ mistakenly identified as Λ's. Many such cases were removed with the help of the particle identification devices. For instance, events with a proton (from an assumed Λ decay) or K^- (from an assumed Ω^- decay) producing light in C_1 or C_2, or having times of flight more than 6 standard deviations from those expected, were rejected. Likewise, events with identified protons from the production vertex were removed. Conversions of $\gamma \rightarrow e^+e^-$ were readily identified by the fact that, for such events interpreted as $\Lambda \rightarrow \pi^- p$ the cosine of the angle between p and Λ in the Λ rest frame peaked sharply at values above 0.97.

3.4 Final Samples

After these cuts the Ξ^- signal (15,570 $\pm$ 150 events above 7,300 background) was very clear in the $\Lambda\pi^-$ mass plot (shaded in Figure 3). Our final Ξ^- sample shown in Figure 4 resulted from requiring a Ξ^- track length of at least 5 *cms*. The fit shown indicated that the peak contained 12,550 $\pm$ 130 events above 960 background,[16] and that the Ξ^- mass (with resolution of 3 MeV/c^2) was $1321 \cdot 4 \pm 0.1$ MeV/c^2, in excellent agreement with the World average.[17]

Because of the much smaller Ω^- production cross section, more stringent geometric requirements were enforced to further reduce the background. Figure 5 shows the ΛK^- mass distribution when the V^- fitted track length was at least 2 *cms*; when Ξ^- candidates were removed; and when both multi-vertex fits were required to have a confidence level greater than 2%. The signal contained 143 $\pm$ 25 events, with a background of about 420 events. To obtain our final Ω^- sample, two further selections were made. First, we required the V^- decay length to be greater than 5 *cms* and less than 3.5 Ω^- lifetimes. We also required that the V^- decay point be removed by at least four standard deviations from the primary vertex. Second, events for which $\cos\theta$—the cosine of the angle between Λ and (ΛK^-) in the (ΛK^-) rest frame—was greater than +0.475 were removed. This

cut removed both the fake background events with small ΛK^- laboratory opening angle where the V^- track length was poorly measured as well as the remaining Ξ^- signal in an unbiased way. The final sample shown in Figure 6 contained 96 ± 15 Ω^- events above 80 background. The fitted ΛK^- mass resolution was 4 MeV/c^2, and the Ω^- mass was 1672.2 ± 0.2 MeV/c^2, in agreement with the World average.[17]

3.5 Background Subtraction

All following plots use background subtracted data samples. In defining these samples, events were chosen which lay within $\pm$ 22 MeV/c^2 of the Ξ^- ($\pm$ 30 MeV/c^2 of the Ω^-) in $\Lambda\pi^-$ (ΛK^-) effective mass. Those events outside $\pm$ 11 MeV/c^2 for the Ξ^- or $\pm$ 15 MeV/c^2 for the Ω^- were weighted negatively so as to subtract the effects of background under the respective peaks. These subsamples of signal and control band events are, respectively, line-shaded and dotted regions in Figures 4 and 6. The distribution of ($\Xi^-\pi^+$) effective mass combinations made in this way is shown in Figure 7 in the low mass region. A clear Ξ° (1530) signal is seen which has a fitted mass and width (not correcting for the resolution of 6 MeV/c^2) of 1532.1 $\pm$0.4 and 17 ± 1 MeV/c^2 respectively. It contains 1244 $\pm$ 50 events above background. Our Ξ° (1530) sample was chosen from a mass band $\pm$ 40 MeV/c^2 from 1532 MeV/c^2, where events outside the $\pm$ 20 MeV/c^2 range were used for purposes of background subtraction.

4. Cross Sections

4.1 Monte Carlo Simulation

In order to compute the total acceptance of the spectrometer, including the reconstruction program and the above selection criteria, a large number of events corresponding to Ξ^-, Ω^- and Ξ° (1530) production were generated (the "thrown" Monte Carlo sample), and subjected to a computer simulation of conditions in

the experiment and hardware including software requirements. Those surviving (the "passing" Monte Carlo sample) were an indication of the overall acceptance for production and decay of these particles. In this process, for example, "raw" data similar to that from a real Ξ^- event would be simulated by computer propagation of all associated particles, from their appropriate vertices, through the known magnetic field and geometric arrangement of detectors in the LASS spectrometer. A fake set of coordinates in the tracking chambers, and ADC and TDC readings in the scintillation and Čerenkov chambers, etc., were thus produced. The resulting set of coordinates, etc., were then processed through the same programs and selections as the actual data. Some effects taken into consideration in this simulation included multiple scattering, absorption, resolution of various detectors, energy loss and weak decay probabilities.

4.1.1 Monte Carlo Distributions

The thrown sample needed to simulate:

a) Primary vertex location in the target;

b) Beam momentum vector;

c) Rotation of event about beam axis;

d) Lifetime distributions of decaying particles $(\Omega^-, \Xi^-, \Lambda, K^\circ)$;

e) Decay distributions of these particles;

f) Hyperon production characteristics.

Items a) - d) were readily simulated, using well known properties of the beam and lifetimes for the particles.[17] Hyperon decays - item e) - were generated isotopically in the parent rest frames. Other distributions were found to make rather little difference to the overall acceptance. To simulate the hyperon production characteristics, item (f), we used the 4-momenta for production particles from events in the data samples themselves. In this way, effects of correlations between

these particles, as well as their momentum distributions, were, at least partially, taken into account in our Monte Carlo sample.

4.1.2 Efficiencies

Approximately 40 randomized variations of each data sample event were generated and processed through the spectrometer, as described. The resulting efficiency ϵ (= number passing/number thrown) was found to depend significantly upon three variables defined as:

x	(hyperon momentum in CMS $\div$ maximum possible value $= p_L/p_{max}$)
p_T^2	(square of hyperon transverse momentum)
n	(number of primary charged particles).

Figures 8 (a) and (b) show the efficiencies as functions of x and p_T^2 for the three hyperons being considered here. They are characterized by a significant drop in efficiency at $x < -0.5$ due to low momentum hyperons failing to travel far enough before decaying, and at $x > 0.8$ due to Λ decays occurring beyond the decay fiducial volume defined by the detectors. Variations of ϵ with p_T^2 were much less dramatic, falling slightly with increasing values. The relative efficiencies for primary charged particle multiplicities of $2:4:6$ were approximately $100:75:50$ in all cases.

Each Monte Carlo event was assigned a weight w (normalized to have mean value = 1.0) given by

$$w(x, p_T^2, n) \;\propto\; \epsilon^{-1}(x, p_T^2, n) \quad ,$$

so that the distributions of x, p_T^2 and n for the passing Monte Carlo events matched those for the data sample. Various distributions of other quantities then also showed good agreement between the passing Monte Carlo events and the

data – a test of the overall simulation process. For example, Figure 9 compares the proper lifetime distribution for the Ξ^- data with the Monte Carlo prediction (solid line). Similarly, the Ξ^- production vertex position is compared in Figure 10. The resolution of the reconstructed Ξ^- and Ω^- masses from the Monte Carlo events also agreed within a few tenths of an MeV/c^2 with those observed in the data.

4.2 Total Cross Sections

Total cross sections were computed from a combination of factors:

$$\sigma_{TOT} = N \times \left(\frac{1}{\epsilon}\right) \times \left(\frac{1}{v}\right) \times \left(\frac{1}{b}\right) \times \left(\frac{1}{1427}\right)$$

in which

v	was the branching ratio for $\Lambda \rightarrow p\pi^-$;
N	was the number of events in the data above background;
ϵ	$\left(= \sum^{w}_{\text{passing}} / \sum^{w}_{\text{thrown}}\right)$ was the average efficiency; and
b	was the branching ratio for the observed V^- decay mode.

The values used were $b\ (\Xi^- \rightarrow \Lambda\pi^-) = 1.0$; $b\ (\Xi^\circ(1530) \rightarrow \pi^+\Xi^-) = \frac{2}{3}$; $b(\Omega^- \rightarrow \Lambda K^-) = 0.686$; and $v(\Lambda \rightarrow p\pi^-) = 0.642$. The overall normalization was 1427 ev/μb.

Cross sections were also computed as a function of production multiplicity in a similar way using, in the above relationship, the multiplicity dependent efficiencies $\epsilon(n)$ rather than ϵ. The results for Ξ^- , Ξ° (1530) and Ω^- are given in Table III and plotted as functions of K^- momentum in Figures 11 (a), (b), (c) for comparison with other available data. Agreement amongst experiments is generally good. The Ξ^- total cross section is almost independent of beam momentum, while the higher multiplicity cross sections rise sharply. The Ω^- and Ξ° (1530) total cross sections also appear to show little beam momentum dependence near 11 GeV/c.

4.3 INCLUSIVE PRODUCTION CHARACTERISTICS

4.3.1 Particle Multiplicities

The average number of charged tracks $\langle n \rangle$ at the production vertex is summarized in Table III for the data samples reported to date. At a given s, values for this quantity show a clear tendency to smaller values for the higher hyperon masses. Figure 12 shows $\langle n \rangle$ as a function of ℓn(s). There is sufficient data so that a meaningful energy dependance can only be established for the Ξ^- where a simple linear fit in ℓn(s) gives a variation of the form $\langle n \rangle \sim s^{0.46 \pm 0.03}$.

4.3.2 Longitudinal Momentum

It is usual to describe inclusive momentum distributions in terms of the Feynman variable $x = p_L/p_{max}$ and the square of the transverse momentum p_T^2 already referred to in Section 4.1.2. The invariant distribution $F(x)$ is defined as

$$F(x) = \frac{1}{\pi p_{max}} \int E \frac{d^2\sigma}{dx dp_T^2} dp_T^2 \quad ,$$

where p_L and p_T are longitudinal and transverse components of the momentum of the hyperon, respectively, in the overall center of mass system, while p_{max} and E are the maximum possible momentum and energy in this system.

These invariant distributions are tabulated in Table IV and shown for each of the 3 hyperons in Figures 13 (a), 14 (a) and 15 (a). The mean values of x from these distributions, summarized in Table III, are all positive, indicating a substantial amount of hyperon exchange contribution to the production of each of these particles. Data from other energies, where available, are included in Table III and in Figures 13, 14, 15. In the Ξ^- case, there is very little variation with beam energy in the values for $\langle x \rangle$ and also very little variation in the shape of F(x) at different s values, with the possible exception of one point from the 16 GeV/c data near $x = +1$. In general, however, the magnitude of F(x) appears to

Table III

Hyperon Inclusive Production Characteristics

(Units are in GeV/c and μb as Appropriate)

Reaction	K^- Momentum	Approx. # of Events	σ_{TOT}	2 prong	4 prong	6 prong	8 prong	$< n_{ch} >$	$< z >$	$< p_T >$	B(GeV/c^{-2}
$K^-p \to \Xi^- + X$	11 GeV/c*	12,553	133 ± 15	25 ± 6	76 ± 11	29 ± 7	4 ± 3	3.9 ± 0.2	0.24 ± 0.01	0.502 ± 0.005	3.14 ± 0.06
	4.2 GeV/c[1]	5,046	157 ± 8	106.6 ± 5.6	49.6 ± 2.8	0.7 ± 0.2		2.65 ± 0.05	0.24 ± 0.01	0.448 ± 0.003	3.9 ± 0.01
	6.5 GeV/c[4]	440	160 ± 8								
	8.25 GeV/c[2]	8,121	157 ± 10	47.5 ± 3	90.4 ± 5.8	18.8 ± 1.2	0.3 ± 0.1	3.64 ± 0.04	0.24 ± 0.01	0.512 ± 0.003	3.09 ± 0.33
	10 GeV/c[3]	876	172 ± 20	38 ± 9	101 ± 15	31 ± 8	2 ± 2	4.0 ± 0.01	0.23 ± 0.04	0.52 ± 0.01	3.1 ± 0.2
	14.3 GeV/c[5]		127 ± 9	14 ± 2	63 ± 6	44 ± 6	6 ± 3	4.7 ± 0.2	0.16 ± 0.05	0.44 ± 0.04	
	16 GeV/c[3]	861	135 ± 15	18 ± 5	61 ± 9	47 ± 3	9 ± 4	4.7 ± 0.01	0.22 ± 0.02	0.59 ± 0.01	2.6 ± 0.1
$K^-p \to \Xi^0(1530) + X$	11 GeV/c*	1,244	44 ± 6	5 ± 2	22 ± 4	17 ± 4	1 ± 1	4.1 ± 0.2	0.09 ± 0.02	0.55 ± 0.03	2.6 ± 0.2
	4.2 GeV/c[1]		30 ± 3						0.09 ± 0.01		
	6.5 GeV/c[4]		38 ± 3								
	8.25 GeV/c[2]	2,772	45 ± 3						0.16 ± 0.03	0.51 ± 0.02	2.59 ± 0.06
	10 GeV/c[3]		43 ± 7	3 ± 3	23 ± 5	1 ± 1			0.13 ± 0.05	0.55 ± 0.02	2.8 ± 0.4
	16 GeV/c[3]		32 ± 5	1 ± 1	18 ± 4	11 ± 3	2 ± 1		0.10 ± 0.05	0.63 ± 0.02	2.0 ± 0.3
$K^-p \to \Omega^- + X$	11 GeV/c*	96	3.9 ± 0.6	1.2 ± 0.3	2.7 ± 0.5	0.03 ± 0.03	< 0.03	3.2 ± 0.3	0.11 ± 0.04	0.57 ± 0.05	2.3 ± 0.3
	4.2 GeV/c[1]	40	0.5 ± 0.1								
	6.5 GeV/c[4]	15	1.4 ± 0.6								
	8.25 GeV/c[2]	67	2.1 ± 0.3					2.88 ± 0.09	0.19 ± 0.02	0.56 ± 0.03	2.8 ± 0.2
	10 GeV/c[3]		3.7 ± 0.9								
	16 GeV/c[3]		3.2 ± 1.1								

* This Experiment.

Table IV

Invariant x Distributions

x Range		$K^-p \to \Xi^- + X$		$K^-p \to \Omega^- + X$		$K^-p \to \Xi^0(1530) + X$	
Low	High	Weighted # Evts.	F(x) (μb)	Weighted # Evts.	F(x) (μb)	Weighted # Evts.	F (x) (μb)
-0.95	-0.55	35	3.8 ± 1.6	1		6	
-0.55	-0.50	22	7.5 ± 1.8			5	
-0.50	-0.45	44	10.7 ± 1.7	2		11	
-0.45	-0.40	59	10.4 ± 1.5		0.4 ± 0.3	11	1.9 ± 0.7
-0.40	-0.35	85	12.1 ± 1.4			0	
-0.35	-0.30	98	11.2 ± 1.2	9		11	
-0.30	-0.25	130	12.3 ± 1.1			23	
-0.25	-0.20	181	14.4 ± 1.1			20	4.6 ± 1.9
-0.20	-0.15	226	15.6 ± 1.1			12	3.6 ± 1.1
-0.15	-0.10	317	19.1 ± 1.1	19	1.5 ± 0.5	27	3.6 ± 1.1
-0.10	-0.05	367	19.6 ± 1.1			40	6.6 ± 2.2
-0.05	0	449	21.9 ± 1.1			37	5.6 ± 1.9
0	0.05	529	24.0 ± 1.1			41	5.9 ± 2.0
0.05	0.10	565	24.0 ± 1.1	17	1.0 ± 0.4	63	8.3 ± 2.4
0.10	0.15	679	27.4 ± 1.1			69	8.8 ± 1.5
0.15	0.20	727	28.3 ± 1.1			76	9.4 ± 1.6
0.20	0.25	785	29.8 ± 1.1			67	7.9 ± 1.6
0.25	0.30	809	30.3 ± 1.1			61	7.1 ± 1.4
0.30	0.35	802	30.2 ± 1.1	17	0.9 ± 0.3	96	11.0 ± 1.6
0.35	0.40	800	30.6 ± 1.1			94	10.7 ± 1.6
0.40	0.45	703	27.5 ± 1.1			56	6.5 ± 1.5
0.45	0.50	720	29.2 ± 1.1			82	9.4 ± 1.5
0.50	0.55	665	28.2 ± 1.1	22	1.3 ± 0.3	59	6.9 ± 1.4
0.55	0.60	567	25.5 ± 1.1			55	6.6 ± 1.5
0.60	0.65	505	24.5 ± 1.1			36	4.4 ± 1.3
0.65	0.70	449	23.7 ± 1.2	8		40	5.2 ± 1.2
0.70	0.75	356	21.1 ± 1.2			30	4.0 ± 1.0
0.75	0.80	285	19.2 ± 1.2		0.3 ± 0.2	29	4.0 ± 1.0
0.80	0.85	235	18.8 ± 1.3			24	3.6 ± 1.0
0.85	0.90	179	17.7 ± 1.4			12	2.0 ± 0.7
0.90	0.95	117	15.7 ± 1.5	1		10	1.1 ± 0.4
0.95	1.00	52	11.0 ± 1.6			4	

decrease noticeably at all x values as s increases. This is slightly more noticeable at large positive x values where hyperon exchange production would be expected to dominate. Possibly, at higher s, the production of Ξ^- is more the result of Ξ^*, Y^* or even Ω^* decays. Data from the Ω^- and $\Xi^*(1530)$ reactions have, within the statistical uncertainties presented, a behavior consistent with the Ξ^-.

4.3.3 Transverse Momentum

Distributions of p_T^2 (integrated over x) are shown in Figures 13 (b), 14 (b), and 15 (b) for the three hyperons. As observed at other momenta,[1–7] these are well described for p_T^2 values up to 1.0 GeV/c^2 by a distribution of the form:

$$\frac{d\sigma}{dp_T^2} = Ae^{-Bp_T^2}$$

Values for B are summarized for each reaction in the final column of Table III for a variety of momenta, and are characterized by the fact that they show very little dependence upon beam momentum, but decrease with hyperon mass. The major exception to this would appear to be in the Ξ^- data at 4.2 GeV/c,[1] with a value closer to 4 than to 3, except that this value was computed only for events with $x > 0.2$.

Our Ξ^- data, presented in Figure 13 (b), extend to values of p_T^2 up to 3.0 (GeV/c)^2—rather higher than those shown for any other experiments. Above 1.0 (GeV/c)^2 there appears to be some excess of events above the extrapolated expectation from the smaller p_T^2 values.

Very little correlation exists between x and p_T for either Ξ^- or Ξ° (1530) production as demonstrated in Figure 16 where $< p_T >$ is plotted vs. x. Similar correlation distributions have also been observed at 4.2 GeV/c,[1] 8.25 GeV/c,[2] 10 GeV/c and 16 GeV/c.[3] They are characterized by an indication of a drop in the value of $< p_T >$ for x near $\pm$ 1 as might be expected kinematically, but are generally rather flat.

5. Polarization and Weak Decay Parameters of Ξ^-

Nonleptonic weak decays of hyperons are usually described by asymmetry parameters α, β, γ given in terms of isospin changing, opposite parity, partial wave amplitudes S and P (which correspond to s–wave and p–wave, respectively, in $\Xi^- \to \Lambda\pi^-$ decays).

The definitions of α, β, γ are:

$$\alpha = \frac{2Re(S^*P)}{|S|^2 + |P|^2} \tag{5.0.1}$$

$$\beta = \frac{2Im(S^*P)}{|S|^2 + |P|^2} = (1-\alpha^2)^{\frac{1}{2}} \sin\phi \tag{5.0.2}$$

$$\gamma = \frac{|S|^2 - |P|^2}{|S|^2 + |P|^2} = (1-\alpha^2)^{\frac{1}{2}} \cos\phi \tag{5.0.3}$$

$$\text{so that} \quad \alpha^2 + \beta^2 + \gamma^2 = 1 \tag{5.0.4}$$

In general, it is interesting to compare these parameters for different members of any given isospin multiplet as a test of the $\Delta I = \frac{1}{2}$ rule, but the comparison of the two decays:

$$\Xi^\circ(\Xi^-) \to \Lambda\pi^\circ(\pi^-)$$

is particularly interesting since the $\Lambda\pi$ systems are purely isospin 1. This means that not only do final state interactions have similar effects in both cases, but also the isospin decay amplitudes are thereby limited to $\Delta I = \frac{1}{2}$ or $\frac{3}{2}$ (unlike, for example, $\Sigma \to N\pi$ decays where final state interactions are unknown mixtures of isospin $\frac{1}{2}$ and $\frac{3}{2}$ and $\Delta I = \frac{5}{2}$ is also possible). As some discrepancy exists between recent measurements of α_Ξ, it is appropriate to determine this parameter from our sample of Ξ^-.

5.1 ANGULAR DISTRIBUTIONS

In the Ξ^- rest frame, the distribution of Λ momentum ($\vec{\Lambda}$) from the decay

$$\Xi^- \rightarrow \Lambda\pi^-$$

is described in terms of the Ξ^- polarization ($\vec{P}_\Xi$) by;

$$\begin{aligned} F(\Theta) &= 1 + \alpha_\Xi P_\Xi \cos\Theta, \\ \text{where} \quad \cos\Theta &= \hat{P}_\Xi \cdot \hat{\Lambda} \quad \text{(unit vectors)} \quad . \end{aligned} \tag{5.1.1}$$

In this decay, each Λ acquires a polarization $\vec{P}_\Lambda(\Theta)$ which depends upon its emission angle Θ, and whose 3 components are given by[18];

$$\left.\begin{aligned} P_{\Lambda_1} &= -P_\Xi \gamma_\Xi sin\Theta / F(\Theta) \\ P_{\Lambda_2} &= P_\Xi \beta_\Xi sin\Theta / F(\Theta) \\ P_{\Lambda_3} &= (P_\Xi cos\Theta + \alpha_\Xi)/F(\Theta) \end{aligned}\right\} \tag{5.1.2}$$

in a coordinate system with axes $\hat{e}_1$, $\hat{e}_2$, $\hat{e}_3$ defined for each decay as:

$$\left.\begin{aligned} \hat{e}_3 &= \hat{\Lambda} \\ \hat{e}_2 &= \frac{\hat{P}_\Xi \times \hat{\Lambda}}{|\hat{P}_\Xi \times \hat{\Lambda}|} \\ \hat{e}_1 &= \hat{e}_2 \times \hat{e}_3 \end{aligned}\right\} \tag{5.1.3}$$

In the subsequent decay;

$$\Lambda \rightarrow p\pi^-$$

the direction of the proton momentum ($\vec{p}$) in this Λ's rest frame then follows the distribution:

$$\begin{aligned} f(\Theta,\ \Psi) &= 1 + \alpha_\Lambda P_\Lambda(\Theta) \cos\Psi \\ \text{where } \cos\Psi &= \hat{p} \cdot \hat{P}_\Lambda(\Theta) \quad . \end{aligned} \tag{5.1.4}$$

A convenient way to present the data is to show distributions of cos Θ and of the 3 proton direction cosines $\cos\psi_k = \hat{p} \cdot \hat{e}_k \quad (k = 1,\ 3)$. These are shown

in Figures 17 (a)-(d) for our entire Ξ^- sample integrated over all (x, p_T^2) values, with their acceptances indicated by the broken curves. These acceptances are very well determined from over 30,000 passing Monte Carlo events, and show only slight variations, exhibiting no sharp dips or gaps. This is a consequence of the solenoidal symmetry of the LASS spectrometer, and is the reason we are able to make accurate determinations of α_Ξ and also to measure the Φ_Ξ parameter free from significant systematic biases. In particular, the distribution in the variable cos Ψ_3— which is usually used to determine α_Ξ, since its slope should be equal to $\alpha_\Xi \alpha_\Lambda$ independent of Ξ polarization—has an acceptance that varies almost linearly, with a slope which is less than 15% of $\alpha_\Xi \alpha_\Lambda$ and is known to better than 1%.

Each distribution in Figure 17 is expected to exhibit a linear form (after correction for acceptance). Their forms are given by (5.1.1):

$$F(\Theta) \quad = 1 + \alpha_\Xi P_\Xi cos\Theta$$

and:

$$\left.\begin{aligned} f_1(\Psi_1) &= 1 + \tfrac{\pi}{4} P_\Xi \gamma_\Xi \alpha_\Lambda cos\Psi_1 \\ f_2(\Psi_2) &= 1 + \tfrac{\pi}{4} P_\Xi \beta_\Xi \alpha_\Lambda cos\Psi_2 \\ f_3(\Psi_3) &= 1 + \alpha_\Lambda \alpha_\Xi cos\Psi_3 \end{aligned}\right\} \qquad (5.1.5)$$

In addition to measuring α_Ξ, β_Ξ and γ_Ξ, therefore, a determination of the slopes of these distributions could be used to measure P_Ξ and, in view of the constraint (5.0.4), could even measure α_Λ. In our fits, however, we used the value $\alpha_\Lambda = 0.642 \pm 0.013$ quoted in Reference 17.

5.2 Maximum Likelihood Fit

Obviously, a fit to the distributions in $\cos\Theta$ and $\cos\Psi_{1-3}$ (after acceptance correction) to the forms (5.1.1) and (5.1.5) subject to the constraint (5.0.4) would provide a determination of α, β, γ and P for the Ξ^-. To allow for the correlations in acceptance between the various angles, however, we used a likelihood method which we describe below.

The probability for a given Ξ^- event to decay after a proper time t_i with Λ momentum $\vec{\Lambda}_i$ in the Ξ^- rest frame and proton momentum $\vec{p}_i$ in the Λ rest frame is proportional to the product of the distributions (5.1.1) and (5.1.4) and an exponential decay factor that depends on the Ξ lifetime τ.

$$\begin{aligned} W_i(\alpha_\Xi, \beta_\Xi, \gamma_\Xi, P_\Xi; \vec{p}_i, \vec{\Lambda}_i, t_i) &= F(\Theta_i) f(\Theta_i, \Psi_i) exp(-t_i/\tau) \\ &= [1 + \alpha_\Lambda \alpha_\Xi \cos\Psi_3 + \alpha_\Xi P_\Xi \cos\Theta \\ &\quad + \alpha_\Lambda P_\Xi \left(-\gamma_\Xi \cos\Psi_1 \sin\Theta + \beta_\Xi \cos\Psi_2 \sin\Theta + \cos\Psi_3 \cos\Theta\right)] \\ &\quad \times exp(-t_i/\tau) \end{aligned} \tag{5.2.1}$$

Clearly, W is a function of Ξ^- decay parameters and polarization, the Ξ^- lifetime τ and α_Λ. Less obviously, it is also a function of the magnetic moment μ_Ξ of the Ξ^-, since the polarization of each event precesses from its original direction parallel to $(\vec{K}_{Beam} \times \vec{\Xi}^-)$ by an amount proportional to $\mu_\Xi t_i$ before decay. In principal, therefore, this method could be used to determine all these quantities, though we found that, in practice, our data were rather insensitive to μ_Ξ.

Each event occupied a point in phase space (denoted here by a set of kinematic variables ω_i) and had an unknown acceptance A_i (ω_i) and a production distribution $B(\omega_i)$ both of which depended, in general, upon all of the ω_i. The likelihood function for the ensemble of N events in our own sample, therefore

was

$$L = \prod_{i=1}^{N} A_i(\omega_i) B_i(\omega_i) W_i(\alpha_\Xi,\ \beta_\Xi, \gamma_\Xi, \vec{P}_\Xi; \omega_i) \quad . \tag{5.2.2}$$

In the formulation of the extended log likelihood method[19], therefore, it was necessary to maximize L given by;

$$L = \sum_{i=1}^{N} \ell n(A_i) + \sum_{i=1}^{N} \ell n(B_i) + \sum_{i=1}^{N} \ell n(W_i) - M \quad , \tag{5.2.3}$$

where $\mathrm{M} = \int A(\omega) B(\omega) W(\omega) d\omega$ over all phase space,

with respect to our parameters.

Detailed knowledge of the functional behavior of $A(\omega)$ and $B(\omega)$ was not required. The first two sums over $\ell n(A)$, and $\ell n(B)$ in this quantity were constants, independent of our parameters. They were, therefore, ignored (actually set to zero) in the optimization process. Evaluation of the integral M was made possible by using the entire thrown Monte Carlo sample which, after weighting as described in Section 4.1, had a distribution $B(\omega)\ \exp(-\mathrm{t}/\tau)$ over phase space. Events which passed our cuts were assigned an acceptance $A = 1$, and $A = 0$ if they failed.

In this way, we calculated;

$$M = \int A(w) B(w) W(w) dw = \frac{1}{T} \sum_{j=1}^{P} w_j W_j \exp(+\mathrm{t_j}/\tau) \tag{5.2.4}$$

where

T was the sum of weights of all thrown (passing and failing) Monte Carlo events;

P was the number of passing Monte Carlo events;

w_j, t_j were the weight and proper time, respectively, of the j^{th} passing Monte Carlo event.

Two further complications were, first, that our data sample actually consisted of weighted events, with weights w that were negative in the background subtraction bands described in Section 3.5; and secondly, that the Ξ^- decay parameters α, β, γ were not independent, but related by equation(5.4). In our fit, therefore, we maximized the function L' (including a Lagrange Multiplier λ) defined by:

$$L' = \sum_{i=1}^{N} w_i \ell n(W_i) - M + \lambda \left(\alpha_\Xi^2 + \beta_\Xi^2 + \gamma_\Xi^2 - 1\right)^2 \qquad (5.2.5)$$

with respect to α_Ξ, β_Ξ, γ_Ξ, and $P_\Xi(x, p_T^2)$.

5.3 Polarization of Ξ^-

In the description in Section 5.2 above, no mention was made of the fact that the parameter P_Ξ was, in fact, a function of x and of p_T^2 for the Ξ^-. In order to make use of our full Ξ^- sample, therefore, we made two fits. In the first, (the "x fit") we treated P_Ξ as if it were only a function of x, with eight possible, discrete values—one for each of eight ranges in x. We fit 11 parameters $[\alpha,\ \beta,\ \gamma,\ P_{x1}, ...P_{xs}]$ using the method described in the preceding section with a value of P_Ξ assigned to each event based upon its placement in one of these x ranges. In the other fit (the p_T fit) a similar division into six p_T ranges was made. In each case, α_Ξ, β_Ξ, γ_Ξ and all P_Ξ values were optimized. In this way, events from different x or p_T regions were all constrained to have the same values for α, β and γ. The distributions resulting from the x fit are shown by the solid curves of Figures 17 (a)-(d) and were obtained by weighting the Monte Carlo events by the function W defined in equation (5.2.1). Very similar curves were obtained from the p_T fit, and clearly provided an excellent description of the data. Results of these two fits are given in Table V.

Table V

Ξ^- Decay Fits

Subsample x Range Low	High	Number of Ξ^- Events	Polarization (%)	α	Φ (Degrees)
−1	-0.5	52	—	—	—
−0.5	-0.2	564	1 ± 10	-0.55 ± 1.6	13 ± 23
−0.2	0	1,259	-4 ± 7	-0.45 ± 0.08	29 ± 75
0	0.3	3,776	-12 ± 5	-0.44 ± 0.04	29 ± 22
0.3	0.4	1,454	-31 ± 6	-0.38 ± 0.06	-15 ± 18
0.4	0.5	1,292	-14 ± 7	-0.40 ± 0.07	-12 ± 35
0.5	0.75	2,268	-30 ± 5	-0.34 ± 0.05	3 ± 14
0.75	1	759	-32 ± 9	-0.39 ± 0.07	19 ± 19
-1	+1	11,424	—	-0.405 ± 0.023	5^{+10}_{-7}
p_T Range (MeV/c) Low	High				
0	115	517	4.5 ± 11	-0.40 ± 0.13	15 ± 45
115	190	784	-4.2 ± 9	-0.41 ± 0.10	12 ± 50
190	315	1,890	-20 ± 6	-0.46 ± 0.06	15 ± 33
315	375	924	-15 ± 9	-0.41 ± 0.08	23 ± 18
375	850	6,200	-22 ± 3	-0.37 ± 0.04	2 ± 11
850	1,500	1,109	-27 ± 7	-0.40 ± 0.07	6 ± 17
0	1,500	11,424	—	-0.404 ± 0.024	6^{+8}_{-11}
Ξ^- Length Cut (cms)					
>5		11,424		-0.40 ± 0.02	5 ± 8
>8		9,066		-0.41 ± 0.03	0 ± 9
>11		7,111		-0.42 ± 0.03	6 ± 12
>14		5,625		-0.42 ± 0.04	-4 ± 16
>17		4,435		-0.44 ± 0.04	0 ± 20

Polarization of hyperons produced by proton collisions in hyperon beams has been observed to grow systematically[20] with increasing p_T^2. This behavior has

also been seen for Ξ^- produced in K^-p collisions at 5 GeV/c,[12] and to a lesser extent at 8.25 GeV/c, [2] with polarization reaching about 45 $\pm$ 5% at p_T = 0.4 GeV/c in the 5 GeV/c experiment. In our data, shown in Figure 18 (a) together with that from the other earlier experiments, an increase in P_Ξ is seen with p_T, but is somewhat more gradual than that observed in the other two experiments. A broader range of p_T values is covered in our measurements, but our polarization only reaches 27 $\pm$ 7 % at p_T = 1.5 GeV/c. The variation which we observed in P_Ξ [Figure 18 (b)] also shows a general trend to increasing P_Ξ with increasing x. Thus, the available data seem to suggest that polarizations at large x or p_T values decrease in K^-p interactions with increasing beam momentum. Our data also show that the magnitude of P_Ξ increases with both p_T and x. This also appears to be the case for the 5 GeV/c experiment but the variation with x in the 8.25 experiment is less obvious.

5.4 Weak Decay Parameters

As a result of the fits described in the previous Sections 5.2 and 5.3, two sets of values of α_Ξ and $\Phi_\Xi (= tan^{-1}\gamma_\Xi/\beta_\Xi)$ were obtained— one in which P_Ξ was regarded as a function of x and the other in which it was regarded as a function of p_T. They are presented in Table V, and are seen to be in excellent agreement.

As a test of the magnitude of systematic errors in our data, and our fitting procedure, various subsamples of events, defined in Table V, were fitted independently. For example, various length cuts were applied to examine the possibility that background might affect our results. We also made various event selections on the basis of both x and p_T. The values of α_Ξ and Φ_Ξ for these subsamples are tabulated in Table V and plotted in Figures 19-21 as functions of x, p_T, and the Ξ^- length cut respectively. Obviously, agreement between subsamples is excellent and dominated by statistical errors. Included in Figures 19 and 20 are our measurements of P_Ξ, and a clear correlation can be seen between smaller uncertainty in Φ_Ξ and large magnitude of P_Ξ. To test the sensitivity of our results to our assumptions regarding background, we also varied the weight we assigned

to the Ξ^- side band events. We varied this w in equation (5.2.5), between its limits of 0 and -1 and produced a variation in α_Ξ of 0.05 without any observable change in Φ_Ξ . The value of -0.36 for w which we have used, arises from our fit to the distribution of $\Lambda\pi^-$ mass in Figure 4, and can be adjusted by $\pm$ 0.3 at most. Including these systematic uncertainties, our best values for decay parameters (taken from the x fit, which also provided estimates of statistical uncertainties), are $\alpha_\Xi = -0.40 \pm 0.03$ and $\Phi_\Xi = 5 \pm 10$ degrees.

5.5 Comparison with Other Results

Parameters obtained from the most recent experimental measurements[10–12] are summarized with our own in Table VI. Values for α_Ξ were recomputed from the ones published using the best value[17] for α_Λ of 0.642 $\pm$ 0.013 on the assumption that the product $\alpha_\Xi\alpha_\Lambda$ should remain unchanged. Values for Φ_Ξ (only measurable in experiments where Ξ^- polarization is evident) are largely unaffected by α_Λ and are tabulated as quoted.

Table VI

$\Xi^- \rightarrow \Lambda\pi^-$ Decay Parameters

Source	Approx. Number of Events Used in Fit	α	Φ (Degrees)
All Experiments Before Ref. 10	25,000	-0.385 ± 0.017	2 ± 6
BNL Hyperon Beam [Ref. 10]	9,046	-0.49 ± 0.04	—
CERN SPS Hyperon Beam [Ref. 11]	150,000	-0.462 ± 0.015	—
BNL-MPS (K^-p) [Ref. 12]	20,865	-0.40 ± 0.03	$14.7 \pm 12.3 \pm 10.0$
This Experiment	11,424	-0.40 ± 0.03	5 ± 10

An odd discrepancy in α_Ξ exists between the hyperon beam results and those from K^-p experiments, the former tending towards larger, negative values. A possible explanation for this discrepancy might arise from the effect of background in the Ξ^- sample referred to above. Such background events display a

decay asymmetry different from that of the Ξ^-, and therefore affect the perceived value for α_Ξ. By adjusting our assumptions regarding the amount of this background (w) between extreme limits, we were able to alter α_Ξ from -0.44 to -0.39. However, in order to make our value agree with either of the hyperon beam results, we would have to assign a value for w greater than 1.0. This would describe an unlikely situation where rather than having a number of Ξ^- events in the dotted regions of Figure 4, the background, itself was actually enhanced exactly in the Ξ^- region. As noted above, we did adjust the actual amount of background in our sample by requiring a variety of different Ξ^- length cuts. This did not, within our model, affect our value for α_Ξ. Most results prior to References 10 and 11 came from K^-p bubble chamber experiments where little background existed, since decay vertices could be clearly observed by human scanners. Both our experiment, and that of Reference 12, also use K^-p induced Ξ^- samples and in both, a noticeable background clearly existed. Its magnitude and effect was, however, easily modelled from the Ξ^- side bands. All these experiments appear to favor similar values of α_Ξ near -0.40.

On the other hand, the experiments described in References 10 and 11 obtained data from hyperon beams where the inherent assumption of no background was made. These experiments obtained values for α_Ξ closer to -0.47 with small errors from the slope of their $\cos\Psi_3$ distributions. The existence of a strongly asymmetric background in their samples, though unlikely, could explain this discrepancy.

From Table VI, we note that the uncertainty in α_Ξ does not decrease as the square root of the number of events in the fit samples, but is ultimately limited by systematic effects, and by the uncertainty in α_Λ. For instance, the two experiments with the greatest precision achieve errors within a factor of 2 from ours, since in our experiment, we experienced relatively little systematic uncertainty, and relatively good statistical precision. Our results, therefore, contribute significantly to the new world average values for $\alpha_\Xi = -0.427 \pm 0.014$ and $\Phi_\Xi = (3.9 \pm 5.2)^\circ$ which can be inferred from Table VI.

5.6 THE $\Delta I = 1/2$ RULE

The ratios $\alpha_{\Xi^0}/\alpha_{\Xi^-} = 0.977$ and $\tau_{\Xi^-}/\tau_{\Xi^0} = 0.484$ can be calculated, after allowing for phase space factors, by assuming that the two decays

$$\Xi^0(\Xi^-) \rightarrow \Lambda\pi^0(\pi^-)$$

proceed with $\Delta I = \frac{1}{2}$ s-wave and p-wave amplitudes (S_1 and P_1) alone. Introducing the possibility of $\Delta I = \frac{3}{2}$ amplitudes (S_3 and P_3) one obtains ratios:[21]

$$\alpha_{\Xi^0}/\alpha_{\Xi^-} = 0.977 + 1.37(S_3/S_1 - P_3/P_1)$$
$$\tau_{\Xi^-}/\tau_{\Xi^0} = 0.484 - 1.44S_3/S_1 - 0.06P_3/P_1$$

Using the new world value for α_{Ξ^-} computed in the previous section, and the best averages for α_{Ξ^0}, τ_{Ξ^-}, τ_{Ξ^0} from Reference 17 we obtain

$$S_3/S_1 = -0.058 \pm 0.015$$
$$P_3/P_1 = -0.051 \pm 0.046$$

indicating some violation of the $\Delta I = \frac{1}{2}$ rule in the s-wave amplitude. We note that if we omit the large negative values for α_{Ξ^-} obtained by the to hyperon beam experiments the calculation above leads to

$$S_3/S_1 = -0.061 \pm 0.015$$
$$\text{and } P_3/P_1 = -0.119 \pm 0.046$$

indicating some $\Delta\pm = \frac{3}{2}$ contribution to both waves.

The major source of uncertainty in P_3/P_1 arises from that in $\alpha_{\Xi^0}/\alpha_{\Xi^-}$. In order to establish any violation of the $\Delta I = \frac{1}{2}$ rule in the p-wave amplitudes, better measurements of both α_{Ξ^-} and α_{Ξ^0} are still required.

6. Search For Higher Mass Hyperon States

Very little information on the production of strange baryons has been accumulated over the last few years. In the most recent review [22] in the 1980 baryon conference, it was noted that the situation of Ξ^* spectroscopy had changed little in four years and that the only well established Ξ^* states were still the $\Xi(1530)$, $\Xi(1820)$ and $\Xi(2030)$. Other narrow states had more recently been reported with masses at 1680 and 2370 MeV/c^2, but confirmation by other experiments was not yet possible. Several other Ξ states which had been reported with masses at 1630, 1940, 2240 and 2420 MeV/c^2 had only been seen with a statistical significance of about 4 standard deviations, or less, in various bubble chamber experiments using K^- beams with momenta less than 5 GeV/c. One of the most interesting strange baryon states observed had been the very narrow, high mass $\sum^+(3170)$ reported[23] to have decay modes only to multi-strange combinations of hadrons such as $\Xi K + \pi$'s, $\sum K\bar{K} + \pi$'s, or $\Lambda K\bar{K} + \pi$'s, etc. All data on these particles were obtained from bubble chambers.

Since the 1980 conference, one bubble chamber experiment[4] and one K^-p counter experiment[24] have reported weak evidence supporting the existence of the $\Xi(2370)$, though the former experiment casts doubt upon its identity as a normal, single Ξ state in view of its peculiar excitation function. This and another counter experiment[25] using a hyperon beam have also presented some evidence in support of the existence of the $\Xi(1940)$, though both signals appear to be less than 4 standard deviations. The latter experiment observed the decay to $\Xi^-\pi^+$, the mode of observation of the earlier bubble chamber experiments. The same experiment also saw evidence for $\Xi(1680)$, but concluded that the most likely spin parity was $\frac{1}{2}^+$ in contrast to the assignment of $\frac{1}{2}^-$ tentatively made by the original authors.[26]

It still appears that the only confirmed Ξ states are the $\Xi(1530)$, $\Xi(1820)$, and $\Xi(2030)$, and that definitive data on all the other states is still required. Given that, with the presently acquired data, our experiment is equivalent to the

largest bubble chamber experiment, it is of interest to search for these states. We find, as expected, evidence for the $\Xi(1530)$ and $\Xi(1820)$ which have known decay modes to Ξ^-, but do not find, as yet, conclusive evidence for other states. In particular, we do not observe the $\Xi(1940)$. Our data also represent the only means available to confirm the existence of the $\sum^+(3170)$ which we fail to do.

6.1 Ξ^* STATES

Figure 22 shows the inclusive $\Xi^-\pi^+$ effective mass distribution over a wider mass range than that in Figure 7. In this, as in all other mass plots shown here, an attempt has been made to distinguish π/K ambiguities using both time of flight and Čerenkov devices. It is a striking fact that, apart from the $\Xi(1530)$, no evidence for Ξ^* resonances is seen in Figure 22. This plot includes all multiplicities, so a certain amount of combinatorial background exists (approximately two combinations, on average, per event). A variety of subsamples, e.g., a specific multiplicity, etc., were examined and none showed any significant signal apart from the $\Xi^\circ(1530)$. One such subsample (shaded events in Figure 22) was chosen by selecting the $\Xi^-\pi^+$ combination in each event for which 4-momentum transfer from K^-_{BEAM} to $\Xi^-\pi^+$ was smallest. The evidence presented in Section 4 suggests that baryons with multiple strangeness appear to be produced by hyperon exchange, prompting this selection. It can be seen, however, that the $\Xi^\circ(1530)$ signal diminishes in strength when this selection is made and indicates that many of the $\Xi^\circ(1530)$ are probably themselves decay products of higher mass states. Earlier experiments, mostly at lower momenta,[17] have reported the existence of a variety of states in this system, usually as four standard deviation effects. The positions at which such states have been reported are indicated on Figure 22. The lack of Ξ^* states decaying to $\Xi^-\pi^+$ is a prediction of a model of baryons based upon two body qq color forces.[27] In this model, the couplings of Ξ^*'s with masses below 2.1 GeV/c^2 to this "elastic" channel are expected to be small with their decays being dominated by "inelastic" $Y\bar{K}$ modes. Our data support this picture. Our small acceptance in the higher mass ranges of the $\Xi^-\pi^+$ spectrum

precludes the possibility of observing anything but very strong signals above 2.1 GeV/c^2.

The only other well established state that we might expect to see in our Ξ^- channels is the $\Xi(1820)$ which has a known decay mode to $\Xi(1530)\pi$. Our mass plot for the Ξ° (1530) π^- system is shown in Figure 23 (with background subtracted as outlined earlier). A clear signal is seen corresponding to the decay of the Ξ° (1820) to $\Xi^\circ(1530)\pi^-$. No other states are seen in this decay mode.

6.2 THE $\sum^+(3170)$ HYPERON

This state is one of the most interesting hyperons to be reported, with high mass, narrow width and unusual decay modes, yet no corroboration of its existence has been possible to date. Data in support of its discovery were originally presented jointly by two experiments[23] to indicate an enhancement of at least six standard deviations at 3.17 GeV/c^2 with width comparable to the resolution of the experiments involved.

The state was seen in the reaction

$$K^- p \rightarrow \sum^+(3170)\pi^- \qquad (6.0.1)$$

at 6.5 and 8.25 GeV/c.

Its characteristics were:

1. Mass 3.17 GeV/c^2 and width compatible with zero.
2. Produced by baryon (Δ) exchange. The distribution of the recoil π^- was characteristically in the backward direction in the center of mass system in the $\sum^+(3170)$ events, while it was in the forward direction in neighboring bins.

3. The $\sum^+(3170)$ decayed only to high multiplicity states with multiple units of strangeness:

$$\sum^+(3170) \rightarrow \Sigma K\bar{K}+ \geq 2\pi$$
$$\rightarrow \Lambda K\bar{K}+ \geq 2\pi$$
$$\rightarrow \Xi^- K + \geq 3\pi$$

and not, for example, simply to Σ or Λ + pions.

4. Neither the $\sum^\circ(3170)$ nor the $\sum^-(3170)$ was seen.

The above observations were made by studying effective masses of the systems listed. Such a study cannot be made with our present data, but it is possible to use our Ξ^- data to search for the above reaction where the $\sum^+(3170)$ decays to $\Xi^- K + \pi$'s by investigating the missing mass recoiling against the slowest π^- in the subsample of events in which we require:

(a) A clean Ξ^-;

(b) At least one π^-;

(c) Two or more additional charged pions or kaons.

The resulting missing mass distribution is shown in Figure 24. This shows all events with the above criteria and with the π^- produced backward in the overall center of mass system. The resolution expected in the $\sum^+(3170)$ region is estimated to be less than 20 MeV, so any signal should be seen in one bin in the plot. In Figure 24 there are five events in the 3.17 GeV bin, about the number expected from a smooth background curve drawn through the region. Using our knowledge of the acceptance for such events, this leads to an upper limit for the cross section for reaction (6.0.1) of 0.07 μb. (95% confidence level).

The cross section for this decay mode of the $\sum^+(3170)$ was $(0.15 \pm 0.07)\mu b$ at 8.25 GeV/c and $(0.3 \pm 0.2)\mu b$ at 6.5 GeV/c. [23] Extrapolation of these cross sections to 11 GeV/c for comparison with our result is obviously model dependent, and statistically uncertain as well, but two extreme cases can be considered. The

most pessimistic would assume that this two body cross section, mediated by $I = \frac{3}{2}$ baryon exchange, might fall with the fourth power of K^- momentum, and gives an 11 GeV/c cross section of $0.05\mu b$. The most optimistic might assume that meson exchange was possible leading to a cross section of about 0.1 μb. The appearance of the signal in the former case is illustrated, as it should appear, in Figure 24. Clearly, our data do not support the existence of the $\sum^+(3170)$, produced with the cross sections measured in Reference 23, but cannot rule out its existence, with production by Δ exchange, at the 95% confidence level. Our data do exclude production of $\sum^+(3170)$ by meson exchange, however.

7. Conclusions

From a study of Ξ^-, Ω^-, and $\Xi^\circ(1530)$ inclusive production from 11 GeV/c K^-p reactions, we can conclude the following:

(i) All three particles are produced predominantly in the forward hemisphere in the CMS, as would be expected if produced by hyperon exchange mechanisms, or if they were daughters of baryon states that were.

(ii) Scaling in the variable x appears to work well at our energy for all three particles.

From the Ξ^- channels we further conclude:

(iii) Polarizations of Ξ^- decrease in magnitude (at large x or p_T^2 values) with increasing beam momentum. In most experiments, a trend in this magnitude is also to increase with both x and p_T.

(iv) A discrepancy exists amongst most recent determinations of the value for α_Ξ. Hyperon beam experiments obtain values below -0.45, but K^-p experiments obtain values closer to -0.40. Our value is -0.40 ± 0.03. Background assumptions affect this result.

(v) Some violation of the $\Delta I = \frac{1}{2}$ rule exists in the s–wave amplitude for $\Xi^- \rightarrow \Lambda\pi^-$ decays. More accurate determinations of α for Ξ° and Ξ^- are needed to make conclusions for the p–wave amplitude.

(vi) We confirm the $\Xi^\circ(1530)\pi^-$ decay mode for the $\Xi^-(1820)$.

(vii) Our data fail to confirm the existence of the $\sum^+(3170)$. We obtain an upper limit for the two-body cross section for production of $\sum^+(3170)$ of $0.07\mu b$ (95% confidence) with subsequent decay to $\Xi K+$ pions.

References

1. S. N. Ganguli, et al., Nucl. Phys. B128, 408 (1977).

   R. J. Hemingway, et al., Nucl. Phys. B142, 205 (1978).

2. M. Baubillier, et al., Nucl. Phys. B192, 1 (1981).

3. P. Sixel, et al., Nucl. Phys. B159, 125 (1979).

4. J. K. Hassall, et al., Nucl. Phys. B189, 397 (1981).

5. C. Louedec et al., Nuovo Cim. 41A, 166 (1977).

   J. M. Gago, Ph.D. Thesis, Univ. of Paris VI (1976).

6. W. Morris, ANL-HEP, C.P. 75-58

7. E. L. Goldwasser and P. F. Schultz, Phys. Rev. D1, 1960 (1970).

8. S. F. Biagi et al., Z. Phys. C9, 305 (1981).

9. R. L. Cool et al. Phys. Rev. D10, 792 (1974).

10. W. E. Cleland et al., Phys. Rev. D21, 12 (1980).

11. S. F. Biagi et al., Phys. Lett. 112B, 265 (1982).

12. J. Bensinger et al., Nucl. Phys. B252, 561 (1985).

13. M. Bourquin et al., Phys. Lett. 87B, 297 (1979).

    M. Bourquin et al., Phys. Lett. 88B, 192 (1979).

    M. Bourquin et al., Z. Phys. C21, 1 (1983).

    M. Bourquin et al., Z. Phys. C21, 17 (1983).

    M. Bourquin et al., Z. Phys. C21, 27 (1983).

    M. Bourquin et al., Nucl. Phys. B241 1 (1984).

14. "The Lass Spectrometer," SLAC-PUB in preparation.

15. D. Aston et al., Nucl. Phys. B247 261 (1984).

D. Aston et al., Phys. Lett. 149B 258 (1984).

16. Fits to mass plots were made using a Breit-Wigner form for mass peaks such as the Ξ^- (actually an approximation to a sum of Gaussian profiles of differing width). The background shape was assumed to have the form:

$$f(M) = (M - M_T)^{\alpha}\exp\,[-\beta(\mathrm{M} - \mathrm{M_T})]$$

where M_T is the threshold mass for system and α, β are fit parameters.

17. Particle Data Group, "Review of Particle Properties," Phys. Lett. 111B, (1982).

18. W. Koch, Reprinted in "Analysis of Scattering and Decay," (M. Nicolic, ed.) Gordon and Breach (1968).

    W. B. Teusch, S. Okubo, E.C.G. Sudarshan, Phys. Rev. 114, 1148 (1959).

19. J. Orear, "Notes on Statistics for Physicists," UCRL-8417, 23 (1958).

20. G. Bunce, et al., Phys. Rev. Lett. 36, 1113 (1976).

    K. Heller, et al., Phys. Rev. Lett. 41, 607 (1978).

    K. Heller, et al., Phys. Lett. 68B, 480 (1977).

    S. Erhan, et al., Phys. Lett. 82B, 301 (1979).

    F. D. Lommano, et al., Phys. Rev. Lett. 43, 1905 (1979).

    K. Raychaudhuri, et al., Phys. Lett. 90B, 319 (1980).

21. O. E. Overseth and S. Pakvasa, Phys. Rev. 184, 1663 (1969).

22. B. T. Meadows, Proceedings of Toronto Baryon Conference, 283 (1980).

23. J. Amirzadeh et al., Phys. Lett. 89B, 125 (1979).

    J. Kinson et al., Proceedings of Toronto Baryon Conference, 278 (1980).

24. C. M. Jenkins et al., Phys. Rev. Lett. 51, 951 (1983).

25. S. F. Biagi et al., Z. Phys. C9, 305 (1981).

26. C. Dionisi et al., Phys. Lett. 80B 145 (1978).

27. N. Isgur and G. Karl, Phys. Rev. D20, 1191 (1979).

N. Isgur et al., Phys. Rev. Lett. 41, 1269 (1980).

Figure Captions

1. Plan View of the LASS Spectrometer.

2. The V^- Topology. Selected events included all possible charge multiplicities and the possible existence of $K^\circ \rightarrow \pi^+\pi^-$ decays in addition to the topology shown.

3. Effective Mass Distribution of $\Lambda\pi^-$ System. The unshaded distribution corresponds to all candidates for the V^- topology. The shaded plot contains only those events that make multi–vertex, geometrically constrained fits, and have satisfactory particle identifications as described in the text. The curves results from a fit described in the text.[16]

4. Final Ξ^- Sample. The $\Lambda\pi^-$ effective mass distribution contains only events after final cuts as described in the text. The line-shaded events clearly contain some background whose effect is monitored by the dotted events in the control regions on either side.

5. $\Lambda\ K^-$ Effective Mass. Events plotted have confidence levels $> 2\%$ for both multi-vertex fits, and a fitted V^- track length of at least 2 *cms*. Events with $M_{\Lambda\pi^-}$ within 11 MeV/c^2 of Ξ^- have been removed.

6. Final Ω^- Sample. Line-shaded and dotted events indicate the signal and side band subtraction regions respectively. The curve comes from a fit described in the text.[16]

7. $\Xi^-\pi^+$ Effective Mass Distribution. Line-shaded and dotted events indicate signal and side band subtraction regions respectively. The curve comes from a fit described in the text.[16]

8. Ξ^-, Ω^- and $\Xi^\circ(1530)$ Acceptances. (a) The acceptance for each hyperon, as a function of x, integrated over p_T^2; (b) acceptance versus p_T^2 integrated over x. The solid curves are for Ξ^-; the dashed curves for $\Xi^\circ(1530)$ and the

dot dashed curves for Ω^-.

9. Ξ^- Lifetime Distribution. The uncorrected lifetime distribution for Ξ^- events shows deviations from linearity due to acceptance effects. The curve represents the Monte Carlo simulation of this distribution.

10. Production Vertex Distribution for Ξ^- Events. The curve represents the Monte Carlo simulation of this distribution.

11. Total Cross Sections. (a) $K^-p \rightarrow \Xi^-$ + anything; (b) $K^-p \rightarrow \Omega^-$ + anything; (c) $K^-p \rightarrow \Xi^\circ(1530)$ + anything. Cross sections are shown as a function of K^- momentum in the laboratory. Where data exist, cross sections for different multiplicities are shown. The values for this experiment are indicated by the solid points. The curves are included to guide the eye only.

12. Mean Charged Multiplicity vs s for the Reactions $K^- \rightarrow \Xi^-$ + Anything and Ω^- + Anything. A fit of the Ξ^- data to the form $\langle n \rangle \propto s^{0.46 \pm 0.03}$ is shown. The dashed line for the Ω^- data is included only to guide the eye.

13. Momentum Distribution for $K^-p \rightarrow \Xi^-$ + Anything. (a) The invariant cross section $F(x)$ vs x is compared with other data. To reduce confusion, error bars are included only for this experiment, whenever they are larger than the dots. Estimates of errors in all plots for this experiment include uncertainties in acceptance. Most error bars are smaller than the dots. The plots come from: this experiment (12,551 events); 16.0 GeV/c (933 events); 8.25 GeV/c (8,121 events); 4.2 GeV/c (5,046 events). (b) $d\sigma/dp_T^2$ vs p_T^2 for this experiment. The curve indicates a fit of the form $d\sigma/dp_T^2 = (411 \pm 6)$ exp $(-3.14 \pm 0.06)p_T^2$.

14. Production Characteristics for $K^-p \rightarrow \Omega^-$ + Anything. (a) $F(x)$ vs x. Error bars are included only for this experiment to reduce confusion. (b) $d\sigma/dp_T^2$ for this experiment. The fit is of the form $d\sigma/dp_T^2 = (13 \pm 3)$ exp $(-2.3 + 0.3)p_T^2$. Plots include 96 events from this experiment and 63 events from the 8.25 GeV/c data.

15. Production Characteristics for $K^-p \to \Xi^\circ$ (1530) + Anything. (a) $F(x)$ vs. x. Error bars are included only for this experiment whenever larger than the dots. (b) $d\sigma/dp_T^2$ for this experiment. The fit is of the form $d\sigma/dp_T^2 = (73 \pm 12)$ exp $(-2.6 + 0.5)p_T^2$.

16. $< p_T >$ vs. x. (a) $K^-p \to \Xi^-$ + anything; (b) $K^-p \to \Omega^-$ + anything; (c) $K^-p \to \Xi^\circ(1530)$ + anything. When available, other published data are included for comparison. Error bars are included only for this experiment where they are larger than the dots.

17. Ξ^- Decay Angles. Distribution of the four angles Ψ_{1-3} and θ defined in the text are shown in (a)-(d) respectively. The solid curves are the result of the "x–fit" described in the text. Dotted curves indicate acceptances in these angles (in arbitrary units).

18. Polarization of Ξ^- from $K^-p \to \Xi^-$ + Anything. (a) as a function of p_T; (b) as a function of x. All available data from other experiments are included in the plots.

19. x Dependence of Ξ^- Decay Parameters. Variations in the values obtained from (a) α; (b) Φ; and (c) polarization are shown as functions of x. Only polarization may show any variation in the absence of systematic effects. Error bars indicate statistical uncertainties only.

20. p_T Dependence of Ξ^- Decay Parameters. Variations in the values obtained for (a) α; (b) Φ; and (c) polarization are shown as functions of p_T. Only polarization may show any variation in the absence of systematic effects. Error bars are purely statistical.

21. Systematic Effects in Ξ^- Decay Parameters. Variations in values obtained for (a) α and (b) Φ are shown as functions of Ξ^- track length cut. Longer length cuts reduce background contamination. Error bars represent purely statistical errors from the fits to the various samples.

22. $\Xi^-\pi^+$ Effective Mass Distribution. All combinations in which the π^+ has particle identification information consistent with a π^+ are plotted unshaded. The shaded events are those combinations (one per event) having the smallest value for $u - u_{min}$, where u is the 4-momentum transfer from the K^- beam to the $\Xi^-\pi^+$ system. Arrows indicate positions at which resonances in this system have been reported. The $\Xi^-(1530)$ peak width is consistent with our mass resolution.

23. $\Xi^\circ(1530)\pi^-$ Effective Mass Distribution. All combinations are plotted. The arrow indicates the position of the $\Xi^-(1820)$ resonances.

24. Missing Mass Opposite the π^-. The event sample is as defined in the text. The curve is a Gaussian peak having a width equal to our resolution centered at 3.17 GeV/c^2 plus a smooth background. The peak size is that expected from $I = \frac{3}{2}$ (baryon) exchange.

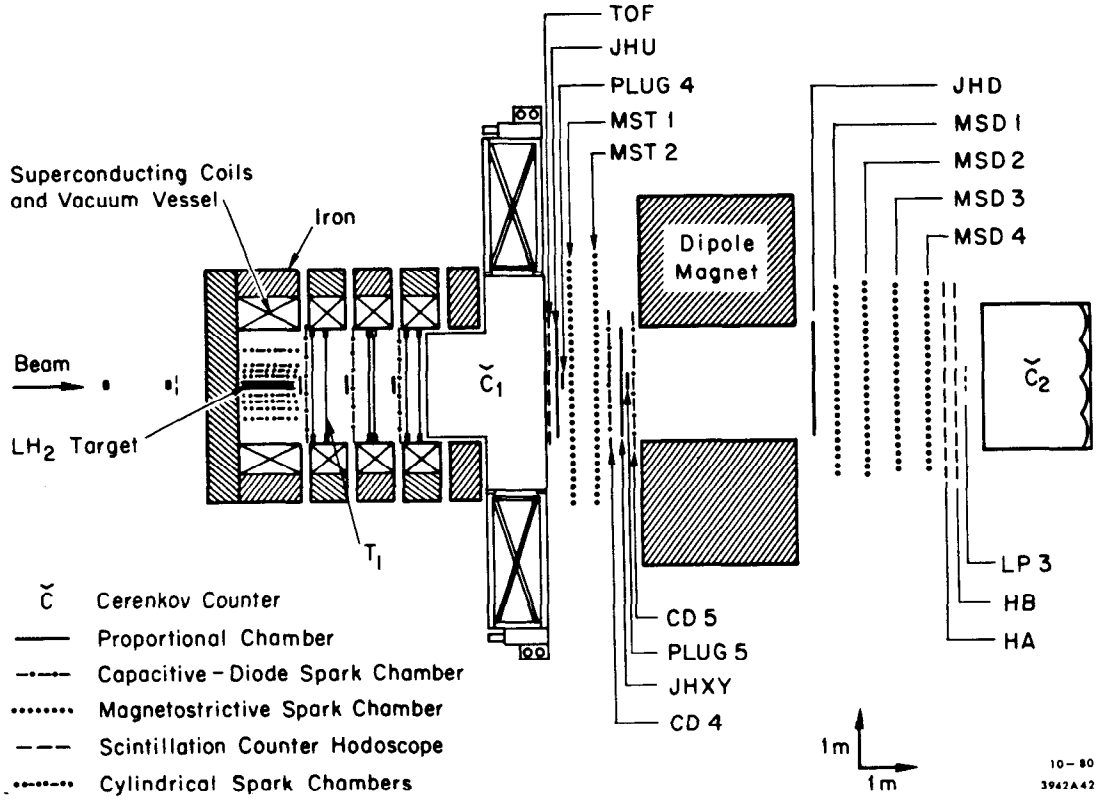
TOF
JHU
PLUG 4
MST 1
MST 2
JHD
MSD 1
MSD 2
MSD 3
MSD 4
Superconducting Coils
and Vacuum Vessel
Iron
Dipole
Magnet
Beam
$\check{C}_1$
$\check{C}_2$
LH_2 Target
T_1
LP 3
HB
HA
CD 5
PLUG 5
JHXY
CD 4
$\check{C}$ Cerenkov Counter
Proportional Chamber
Capacitive-Diode Spark Chamber
Magnetostrictive Spark Chamber
Scintillation Counter Hodoscope
Cylindrical Spark Chambers
1m
1m
10-80
3942A42

Fig. 1

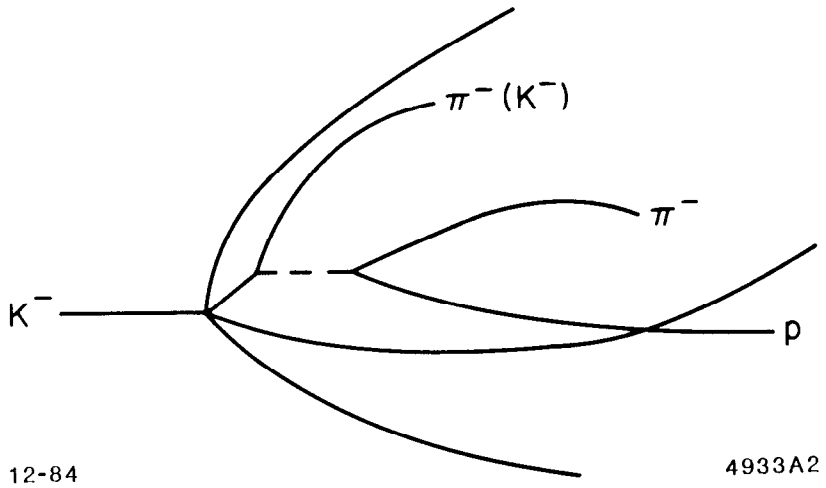

Fig. 2

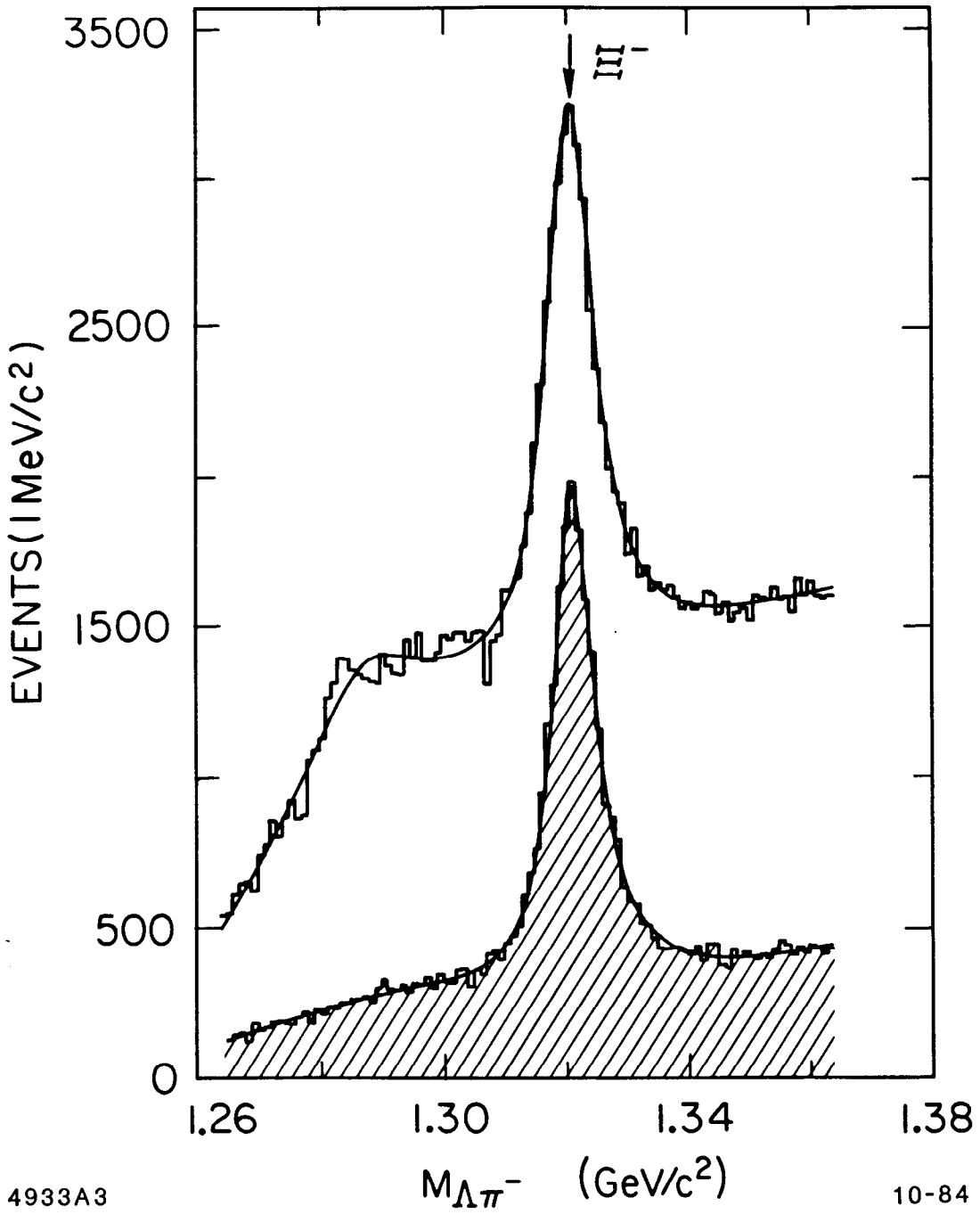
3500
2500
1500
500
0
EVENTS(1 MeV/c²)
Ξ⁻
1.26
1.30
1.34
1.38
MΛπ⁻ (GeV/c²)
4933A3
10-84

Fig. 3

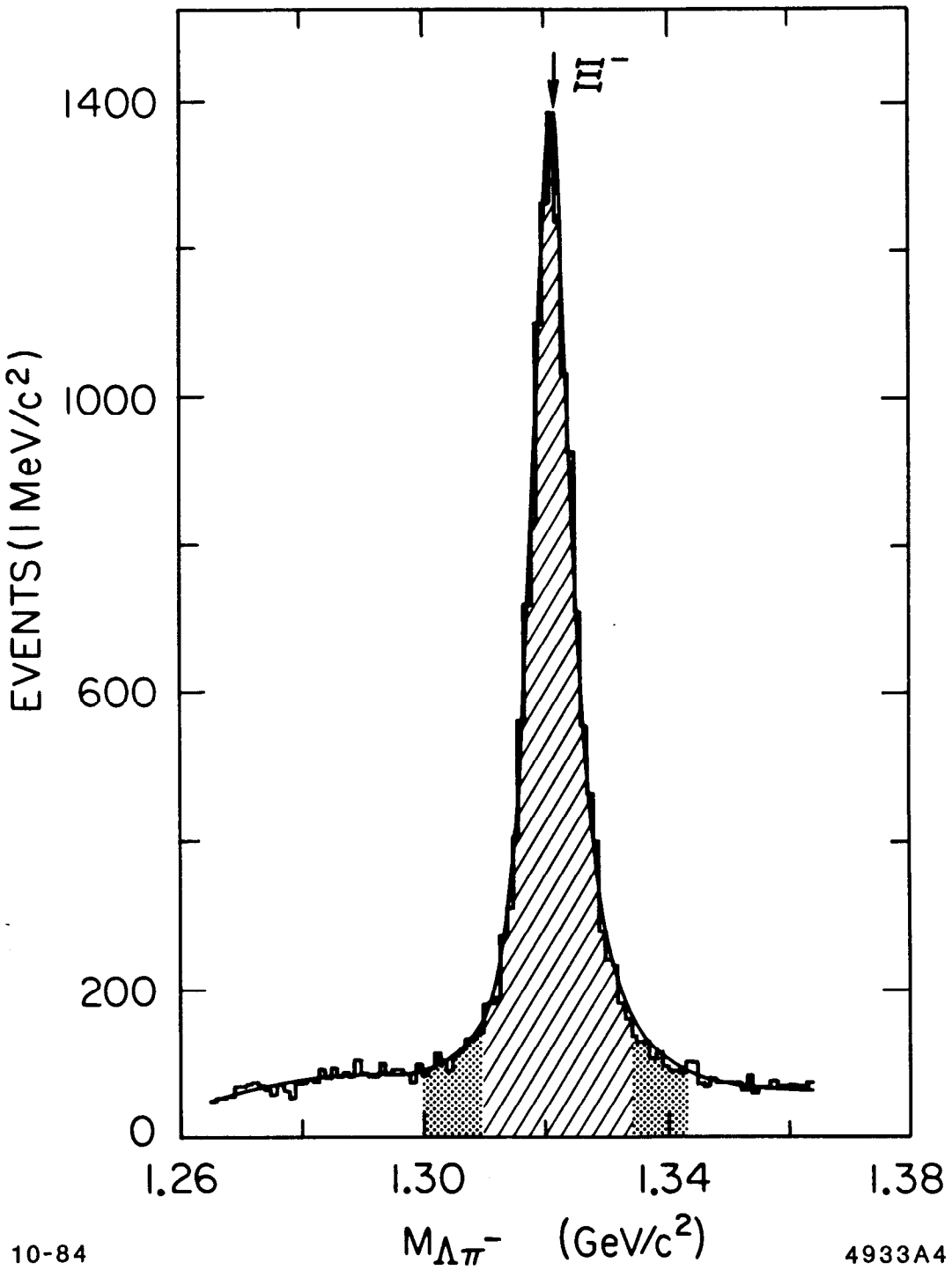
1400
1000
600
200
0
EVENTS(1 MeV/c²)
Ξ⁻
1.26
1.30
1.34
1.38
M_Λπ⁻ (GeV/c²)
10-84
4933A4

Fig. 4

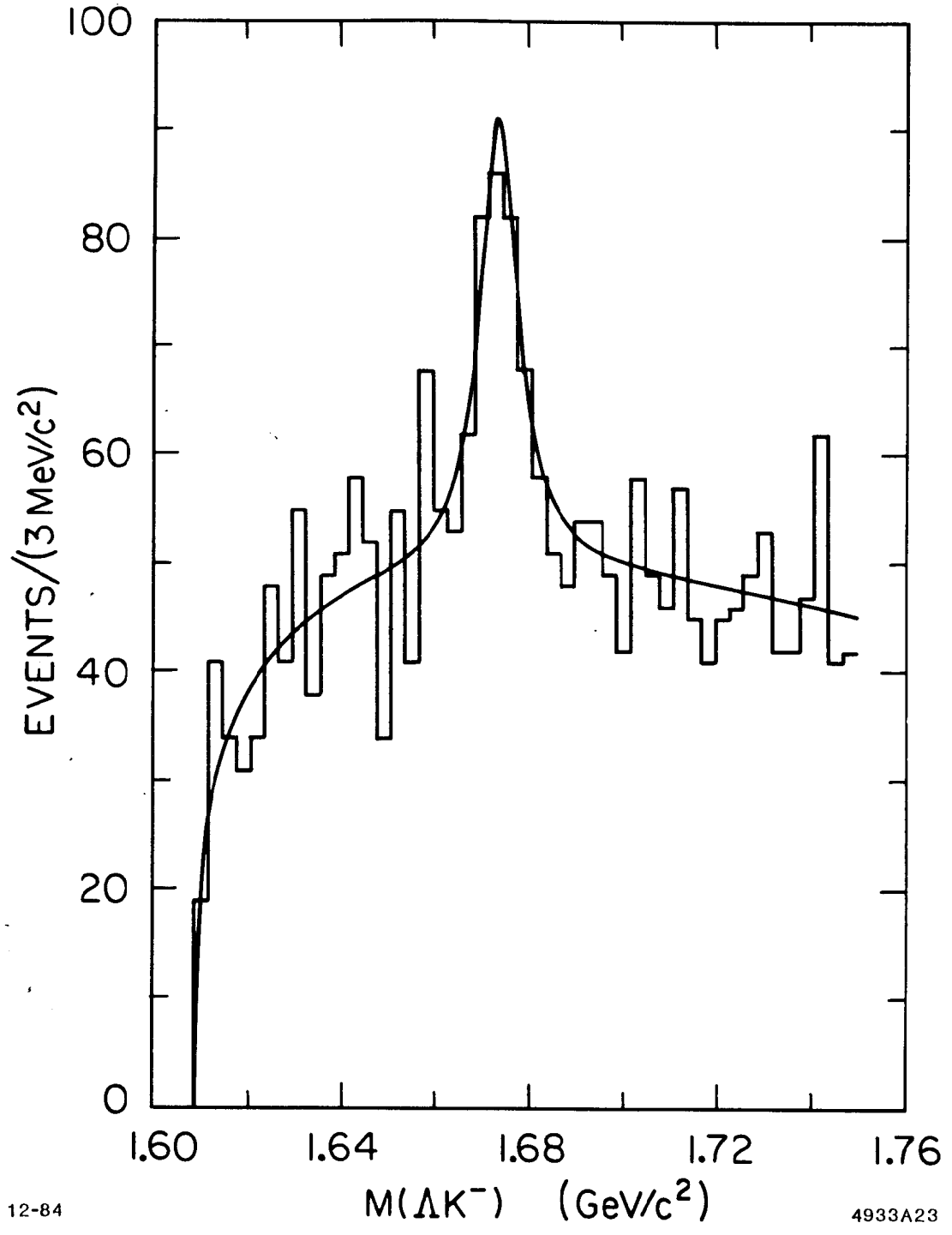
100
80
60
40
20
0
EVENTS/(3 MeV/c²)
1.60
1.64
1.68
1.72
1.76
M(ΛK⁻) (GeV/c²)
12-84
4933A23

Fig. 5

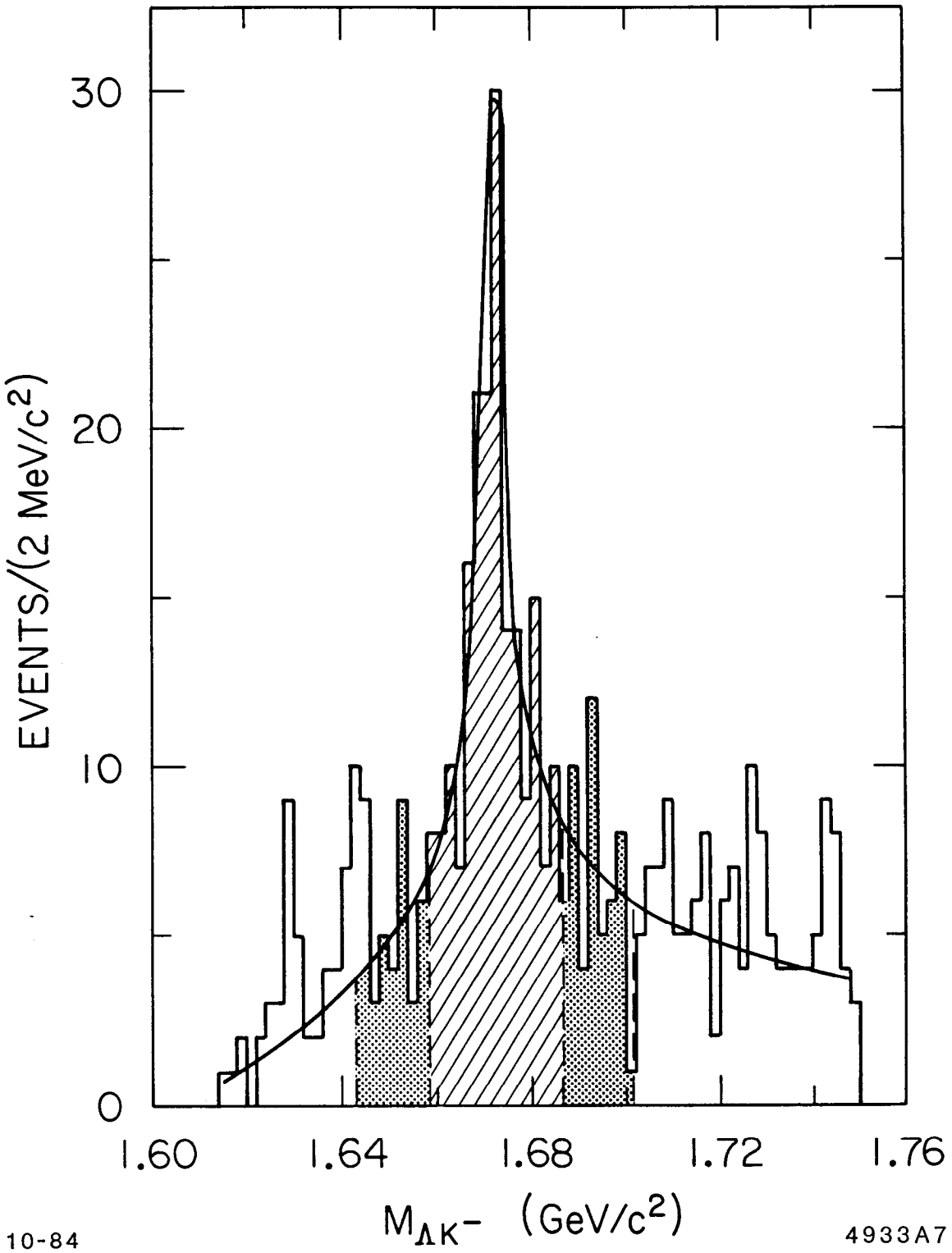
30
20
10
0
EVENTS/(2 MeV/c²)
1.60
1.64
1.68
1.72
1.76
M_ΛK⁻ (GeV/c²)
10-84
4933A7

Fig. 6

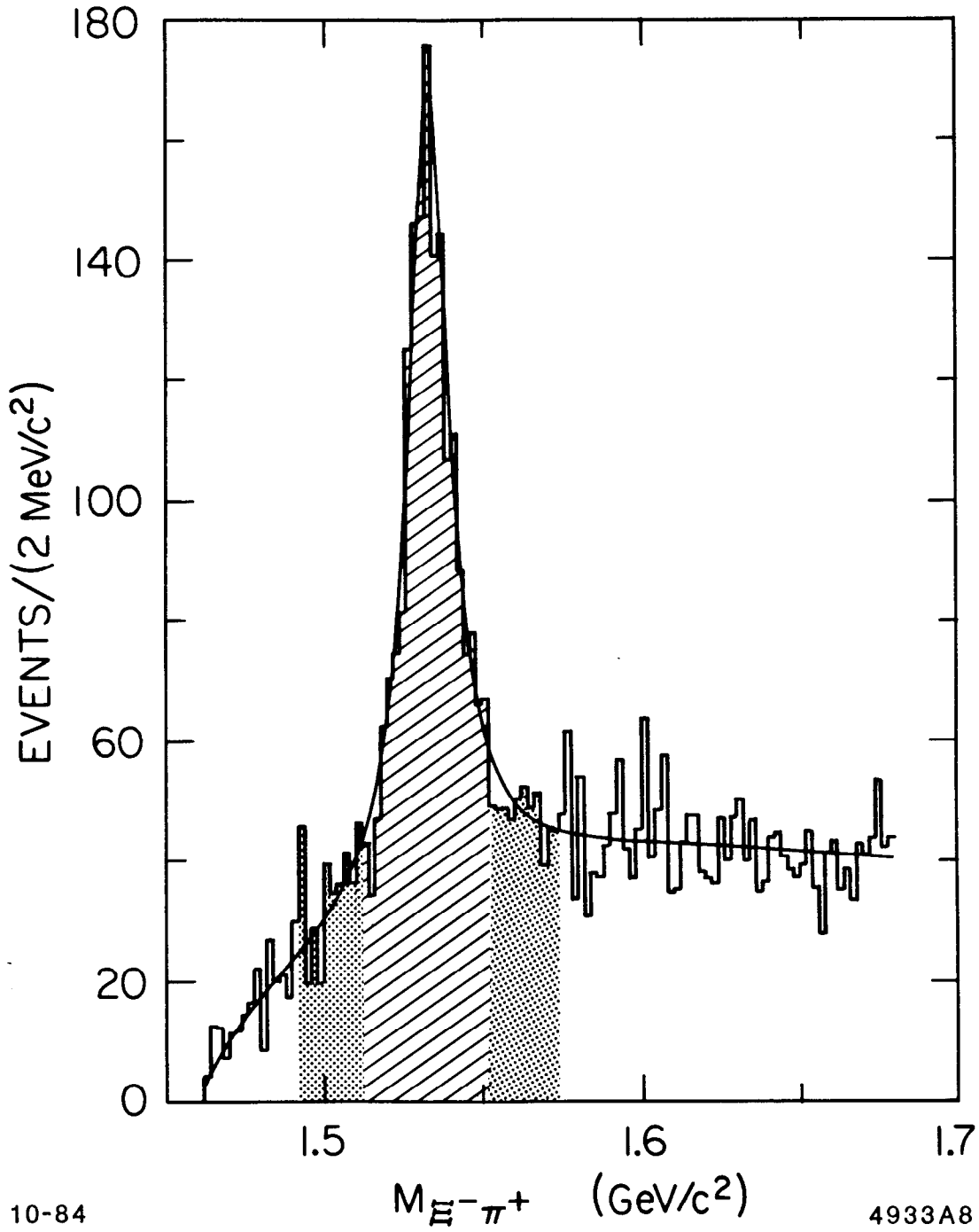
180
140
100
60
20
0
EVENTS/(2 MeV/c²)
1.5
1.6
1.7
M Ξ⁻π⁺ (GeV/c²)
10-84
4933A8

Fig. 7

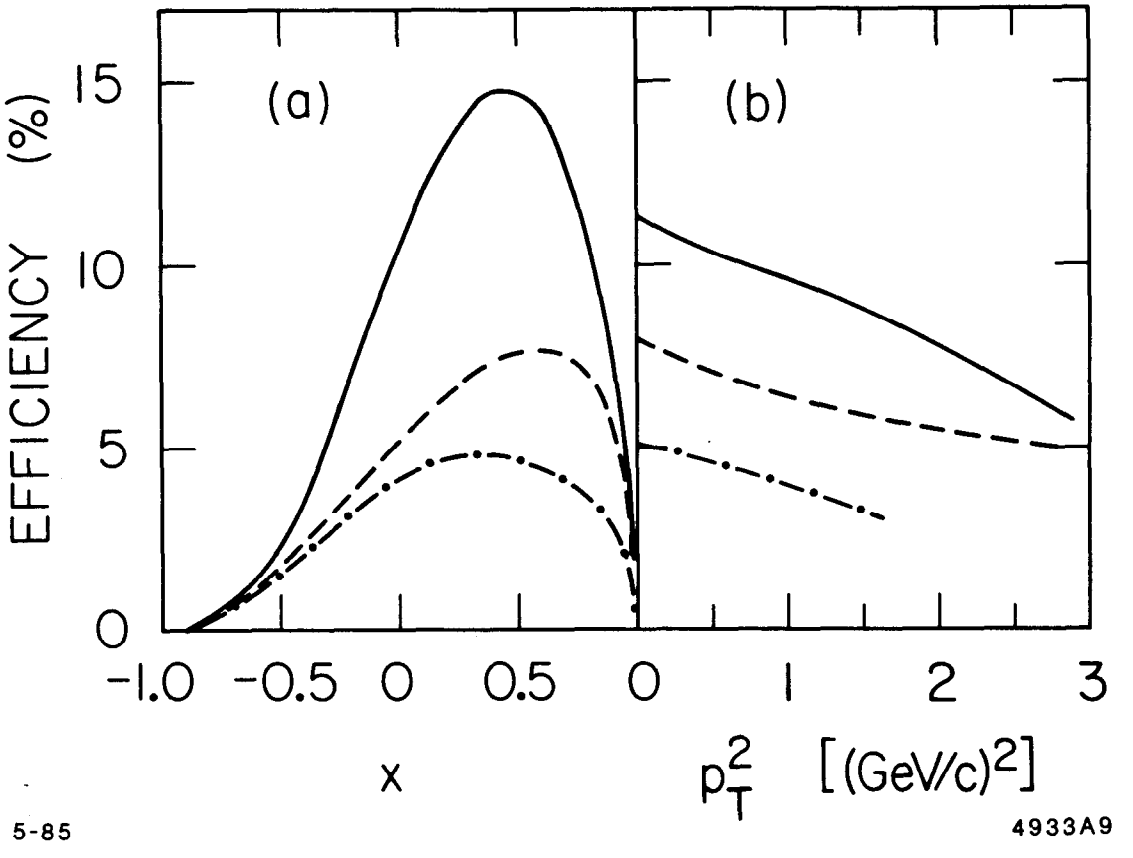

Fig. 8

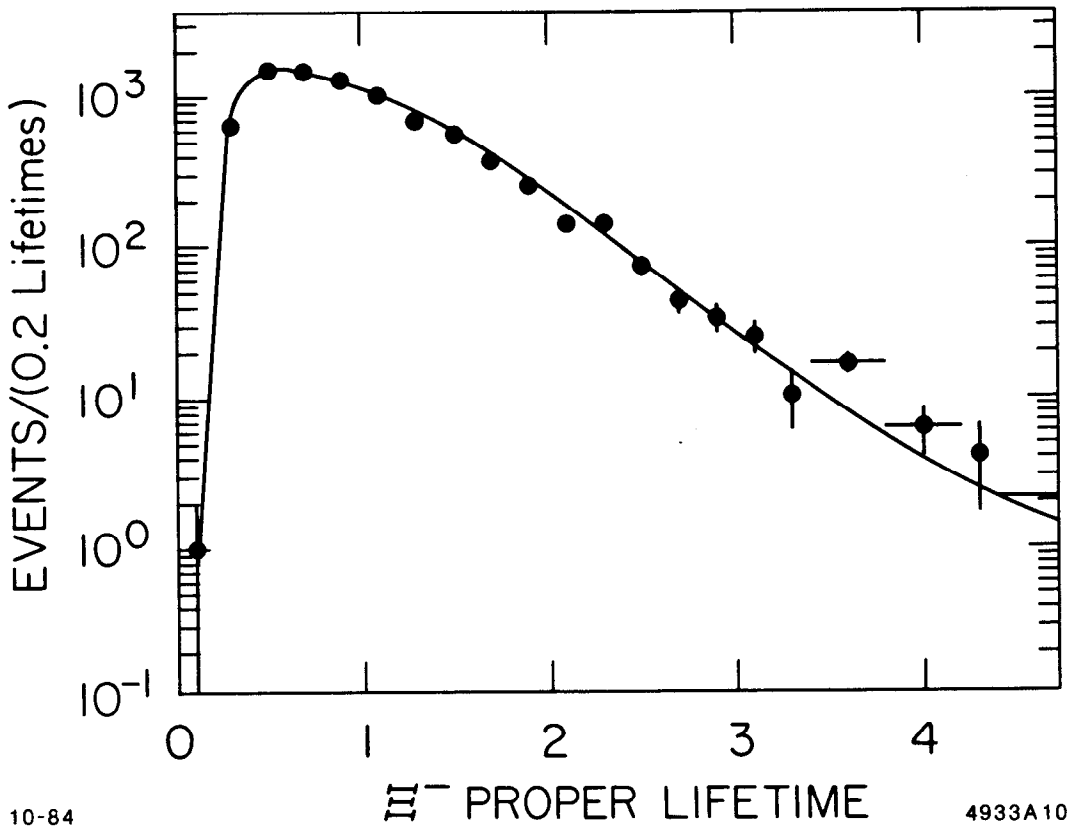
EVENTS/(0.2 Lifetimes)
10^3
10^2
10^1
10^0
10^{-1}
0
1
2
3
4
Ξ^- PROPER LIFETIME
10-84
4933A10

Fig. 9

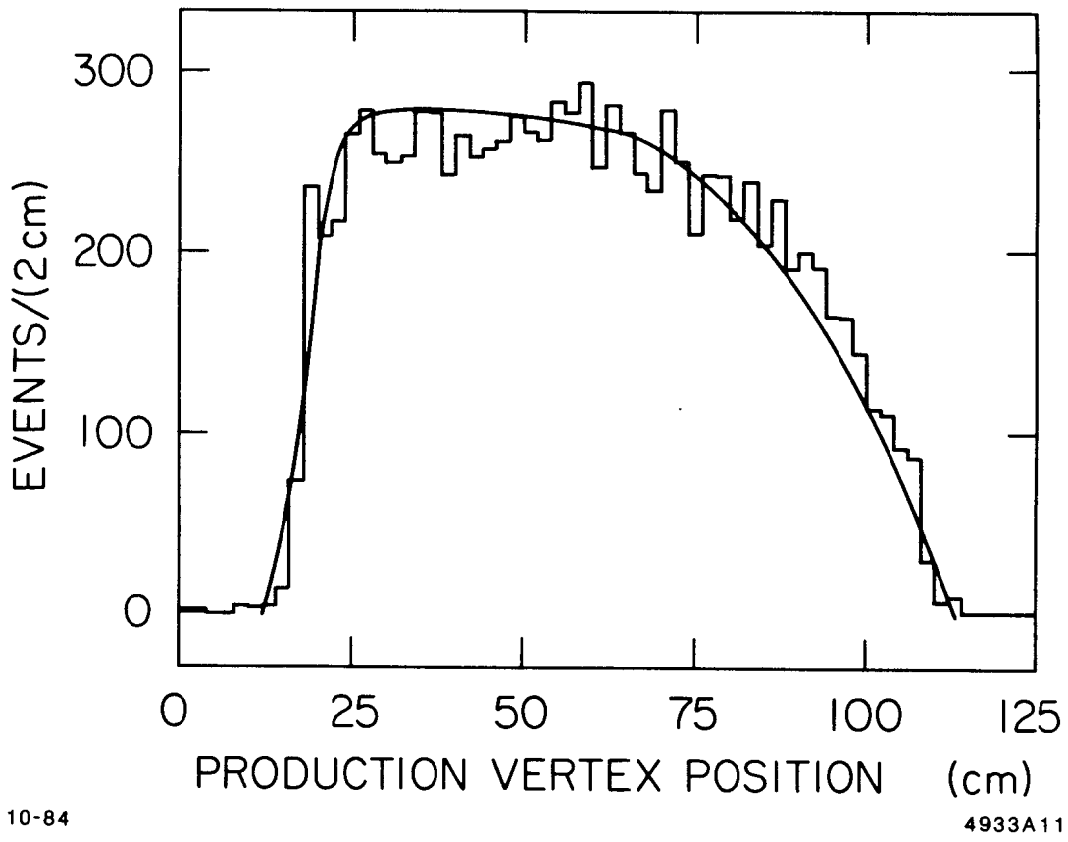
300
200
100
0
EVENTS/(2cm)
0
25
50
75
100
125
PRODUCTION VERTEX POSITION (cm)
10-84
4933A11

Fig. 10

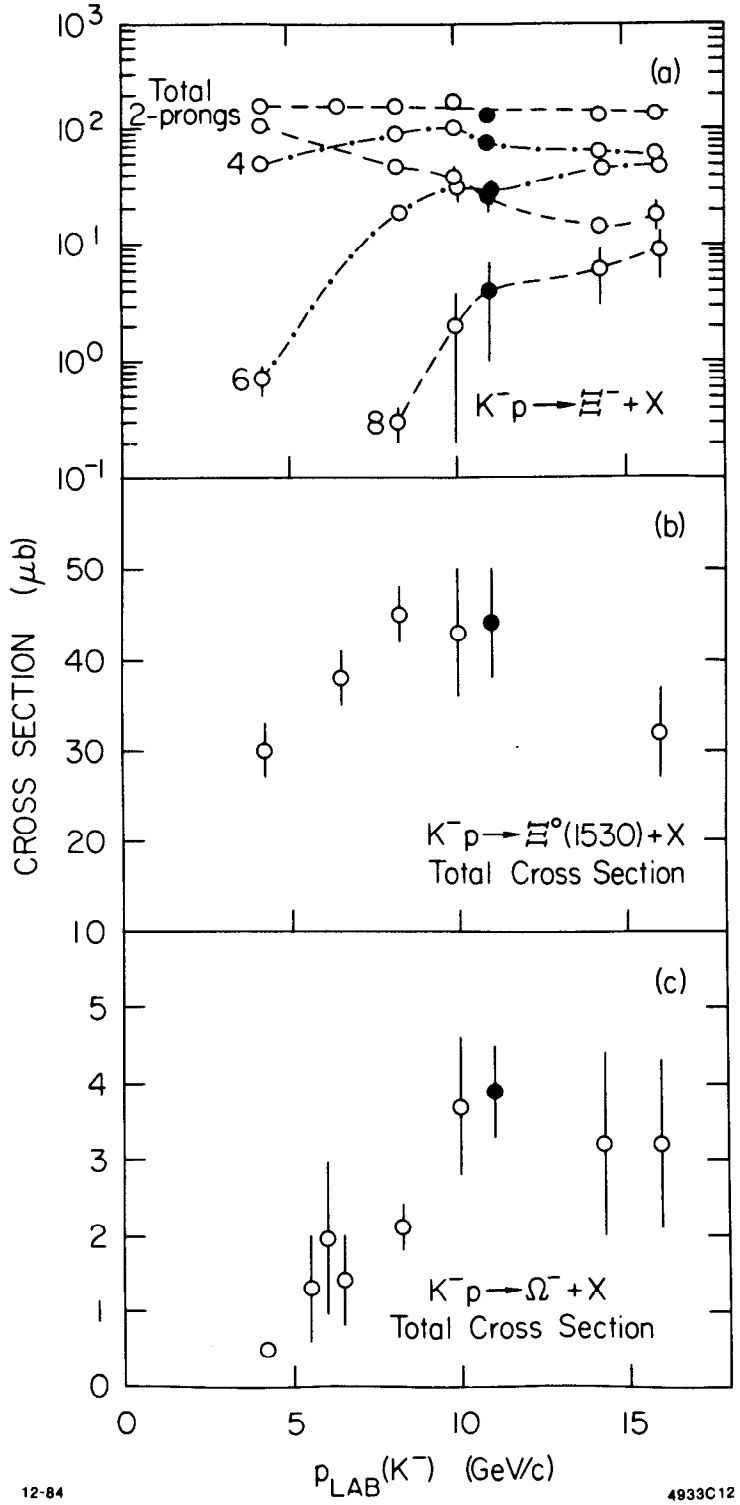
(a)
Total
2-prongs
4
6
8
$K^-p \to \Xi^- + X$
(b)
$K^-p \to \Xi^0(1530) + X$
Total Cross Section
(c)
$K^-p \to \Omega^- + X$
Total Cross Section
CROSS SECTION (μb)
$p_{LAB}(K^-)$ (GeV/c)
12-84
4933C12

Fig. 11

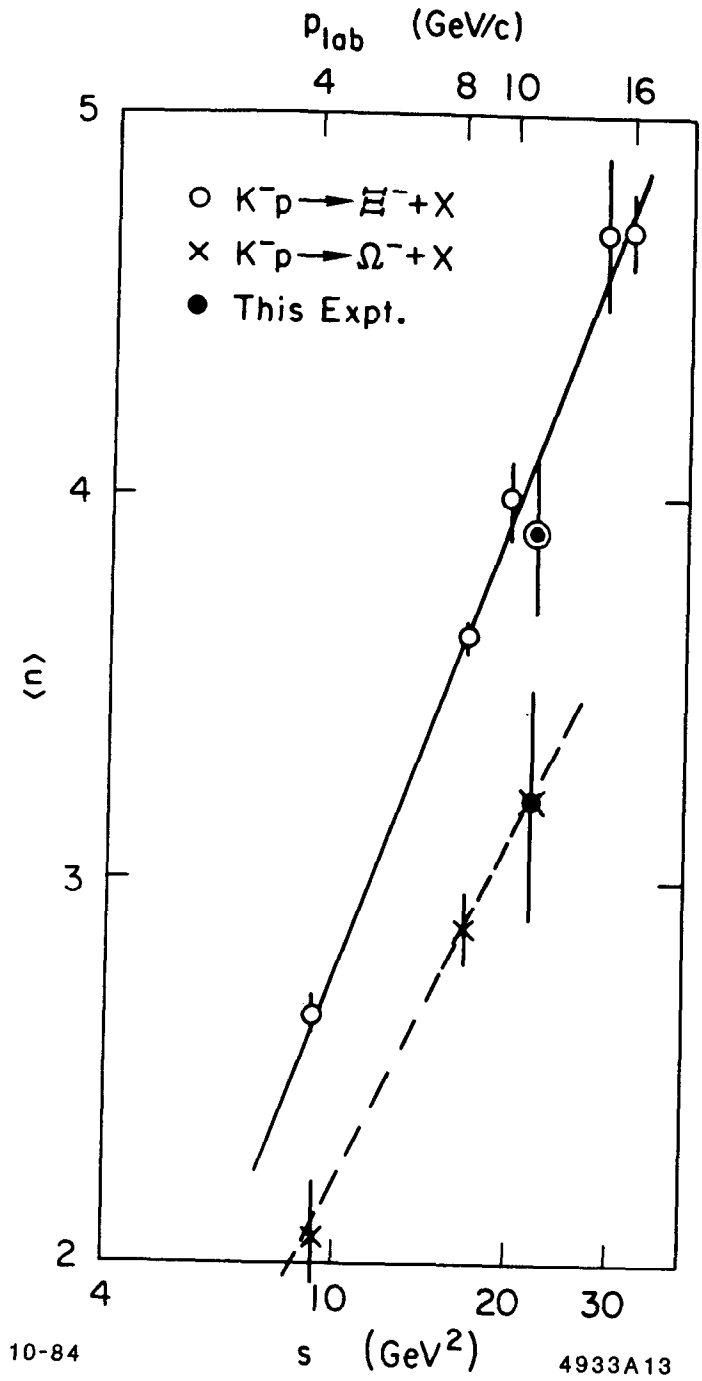
p_{lab} (GeV/c)
4
8
10
16
5
4
3
2
$\langle \xi \rangle$
$K^-p \rightarrow \Xi^- + X$
$K^-p \rightarrow \Omega^- + X$
This Expt.
4
10
20
30
s (GeV^2)
10-84
4933A13

Fig. 12

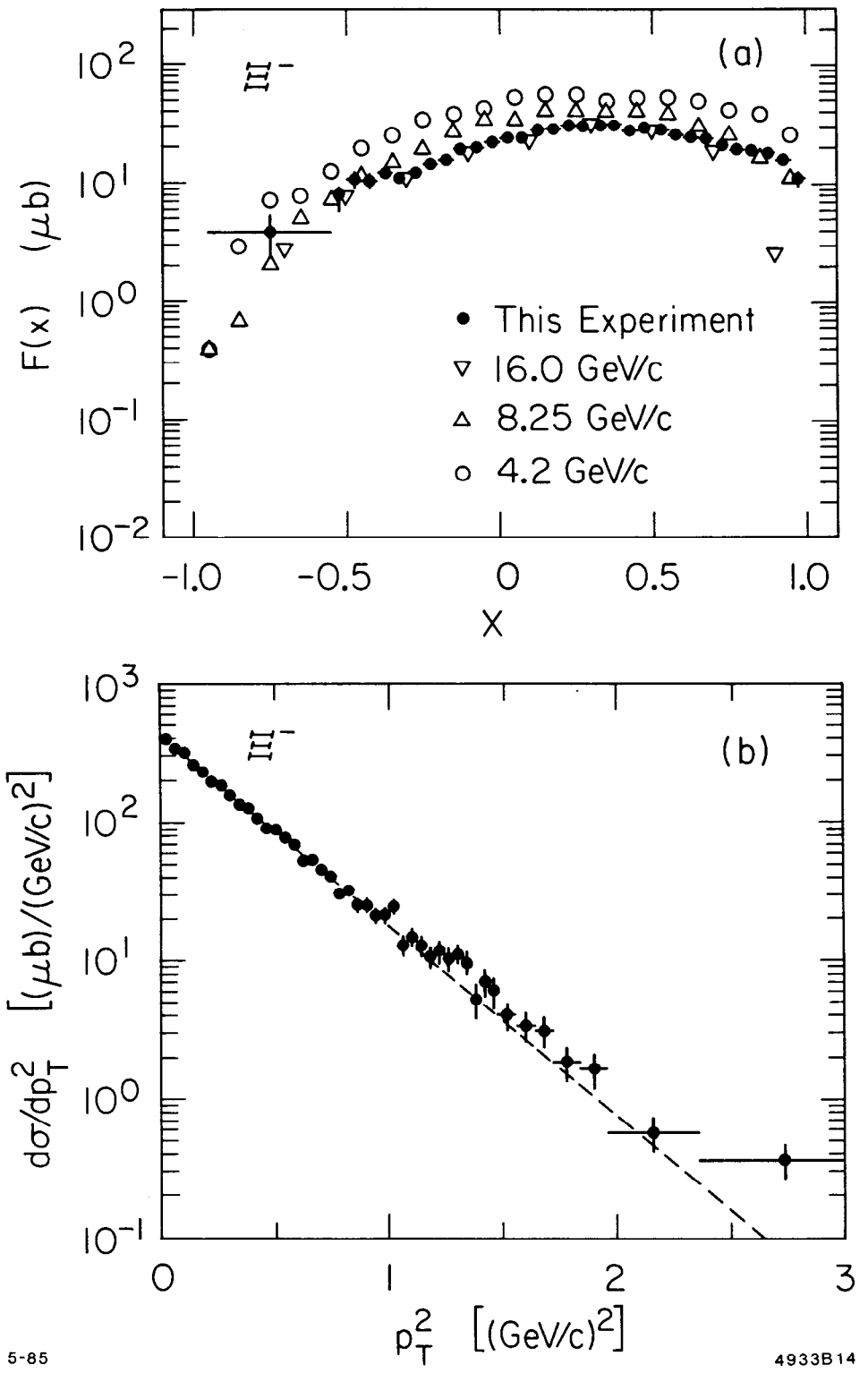
(a)
Ξ⁻
F(x) (μb)
10²
10¹
10⁰
10⁻¹
10⁻²
-1.0
-0.5
0
0.5
1.0
X
This Experiment
16.0 GeV/c
8.25 GeV/c
4.2 GeV/c
(b)
Ξ⁻
dσ/dp²T [(μb)/(GeV/c)²]
10³
10²
10¹
10⁰
10⁻¹
0
1
2
3
p²T [(GeV/c)²]
5-85
4933B14

Fig. 13

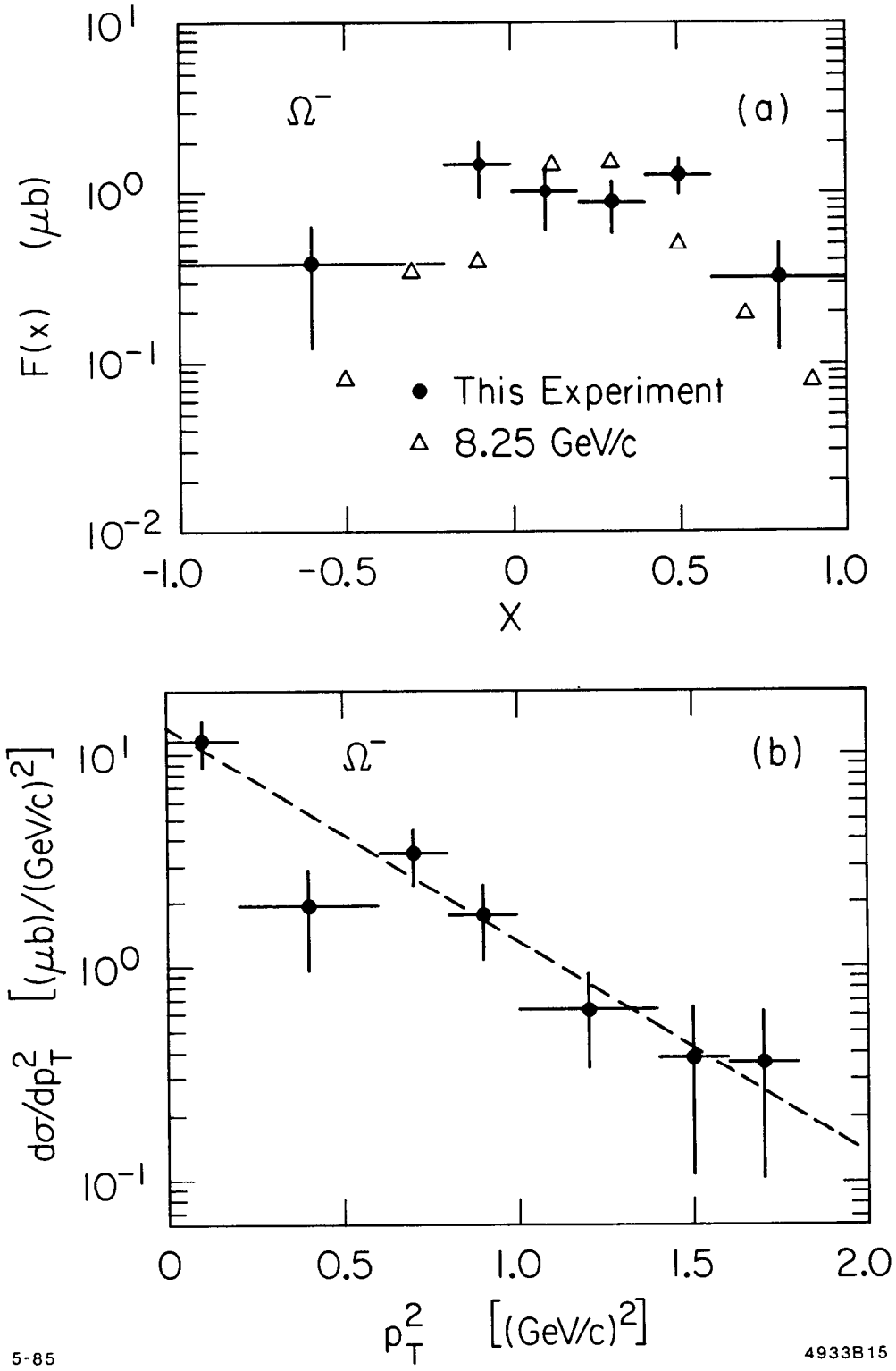
10^1
10^0
10^{-1}
10^{-2}
F(x) (μb)
Ω⁻
(a)
This Experiment
8.25 GeV/c
-1.0
-0.5
0
0.5
1.0
X
10^1
10^0
10^{-1}
dσ/dp²T [(μb)/(GeV/c)²]
Ω⁻
(b)
0
0.5
1.0
1.5
2.0
p²T [(GeV/c)²]
5-85
4933B15

Fig. 14

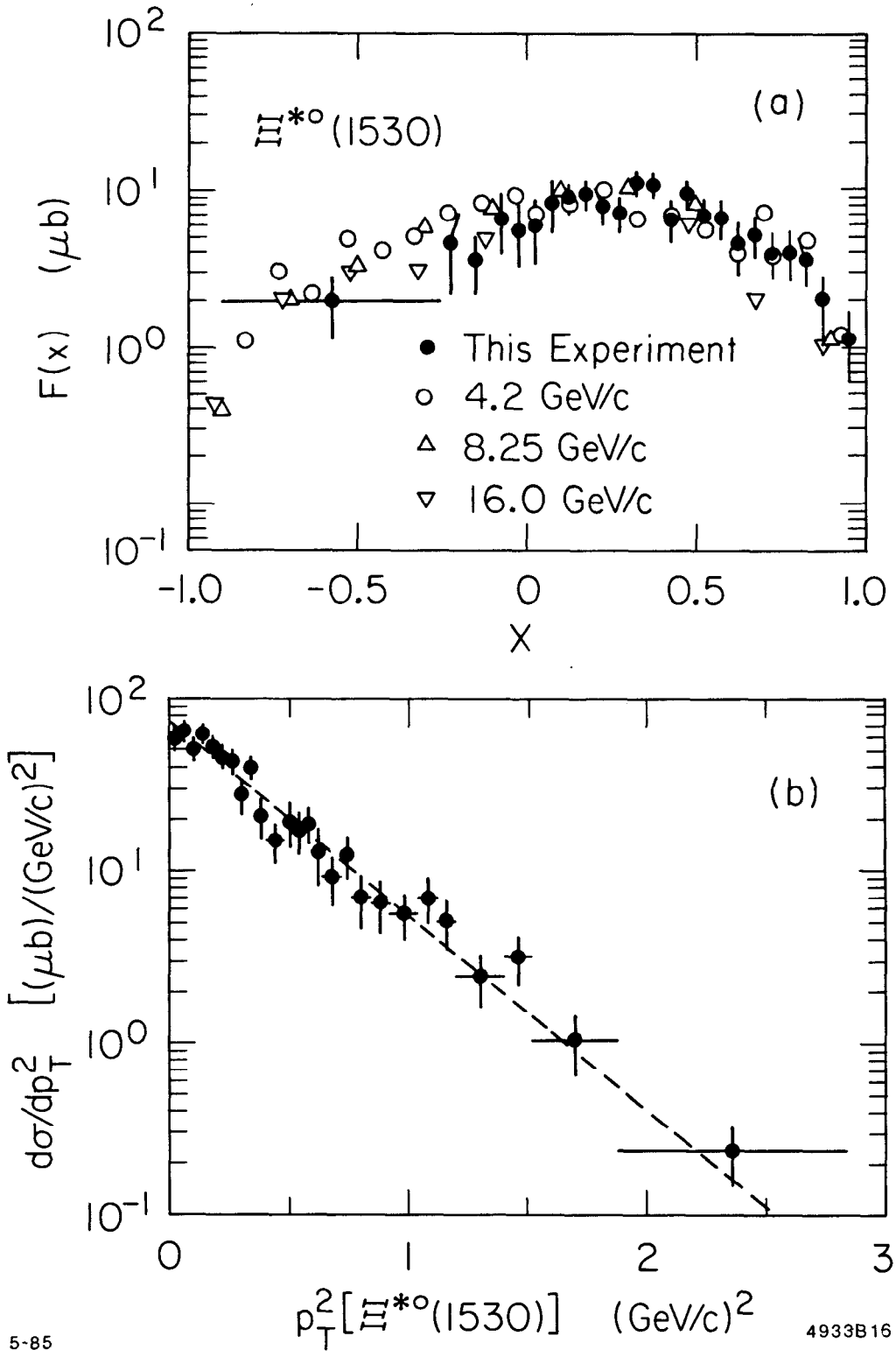
(a)
Ξ*°(1530)
F(x) (μb)
This Experiment
4.2 GeV/c
8.25 GeV/c
16.0 GeV/c
X
(b)
dσ/dp²T [(μb)/(GeV/c)²]
p²T[Ξ*°(1530)] (GeV/c)²
5-85
4933B16

Fig. 15

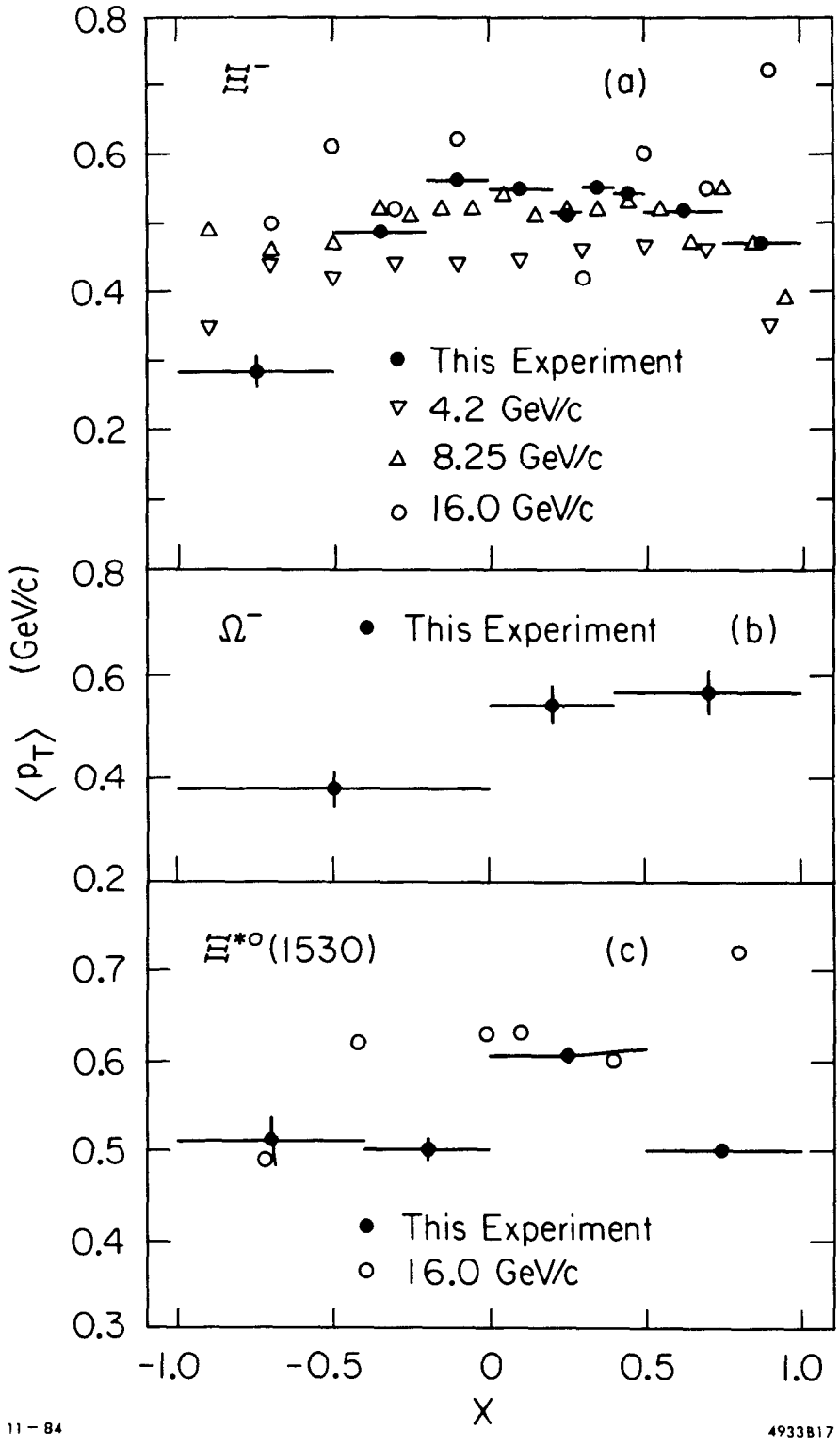
0.8
0.6
0.4
0.2
0.8
0.6
0.4
0.2
0.7
0.6
0.5
0.4
0.3
Ξ^-
(a)
This Experiment
4.2 GeV/c
8.25 GeV/c
16.0 GeV/c
Ω^-
This Experiment
(b)
$\Xi^{*0}(1530)$
(c)
This Experiment
16.0 GeV/c
$\langle p_T \rangle$ (GeV/c)
-1.0
-0.5
0
0.5
1.0
X
11-84
4933B17

Fig. 16

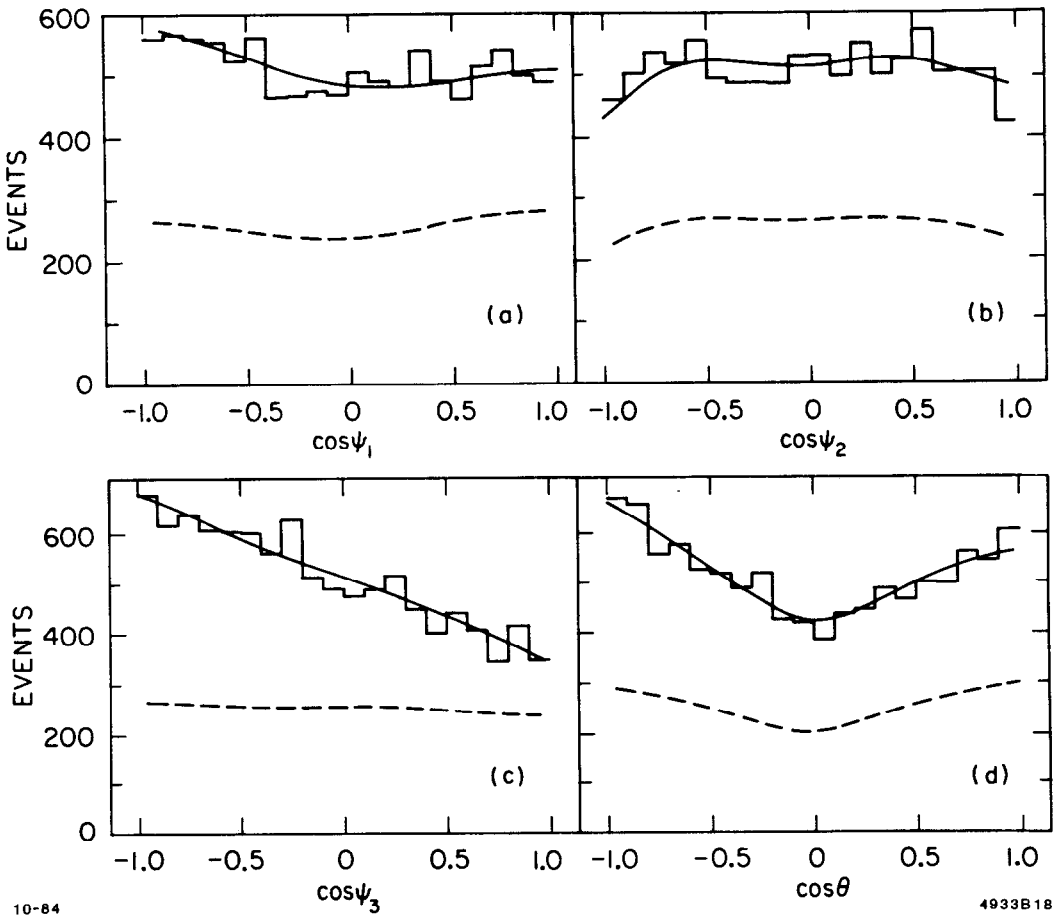
600
400
200
0
EVENTS
(a)
(b)
-1.0
-0.5
0
0.5
1.0
cosψ1
cosψ2
(c)
(d)
cosψ3
cosθ
10-84
4933B18

Fig. 17

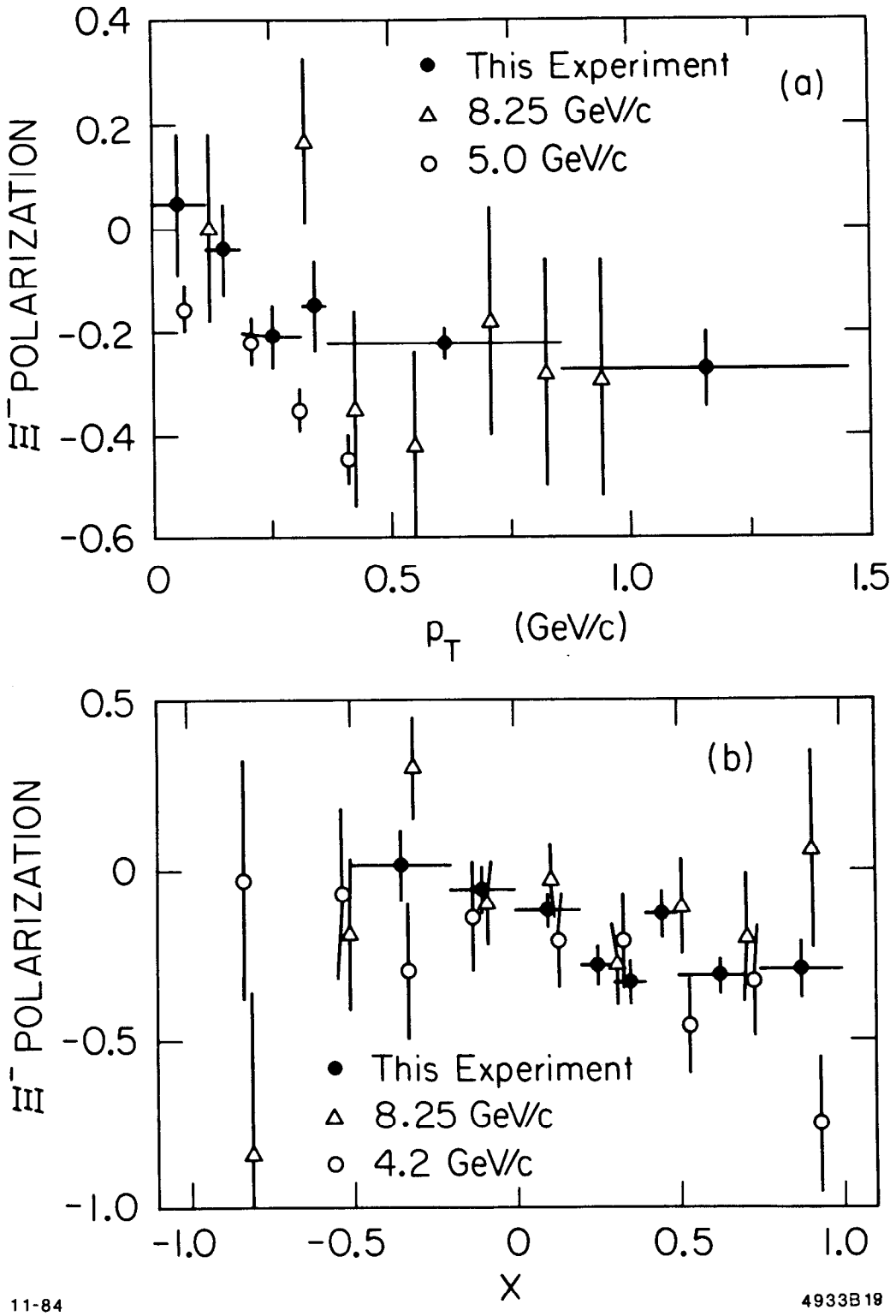
0.4
0.2
0
-0.2
-0.4
-0.6
Ξ^- POLARIZATION
This Experiment
8.25 GeV/c
5.0 GeV/c
(a)
0
0.5
1.0
1.5
p_T (GeV/c)
0.5
0
-0.5
-1.0
$\bar{\Xi}^-$ POLARIZATION
(b)
This Experiment
8.25 GeV/c
4.2 GeV/c
-1.0
-0.5
0
0.5
1.0
X
11-84
4933B19

Fig. 18

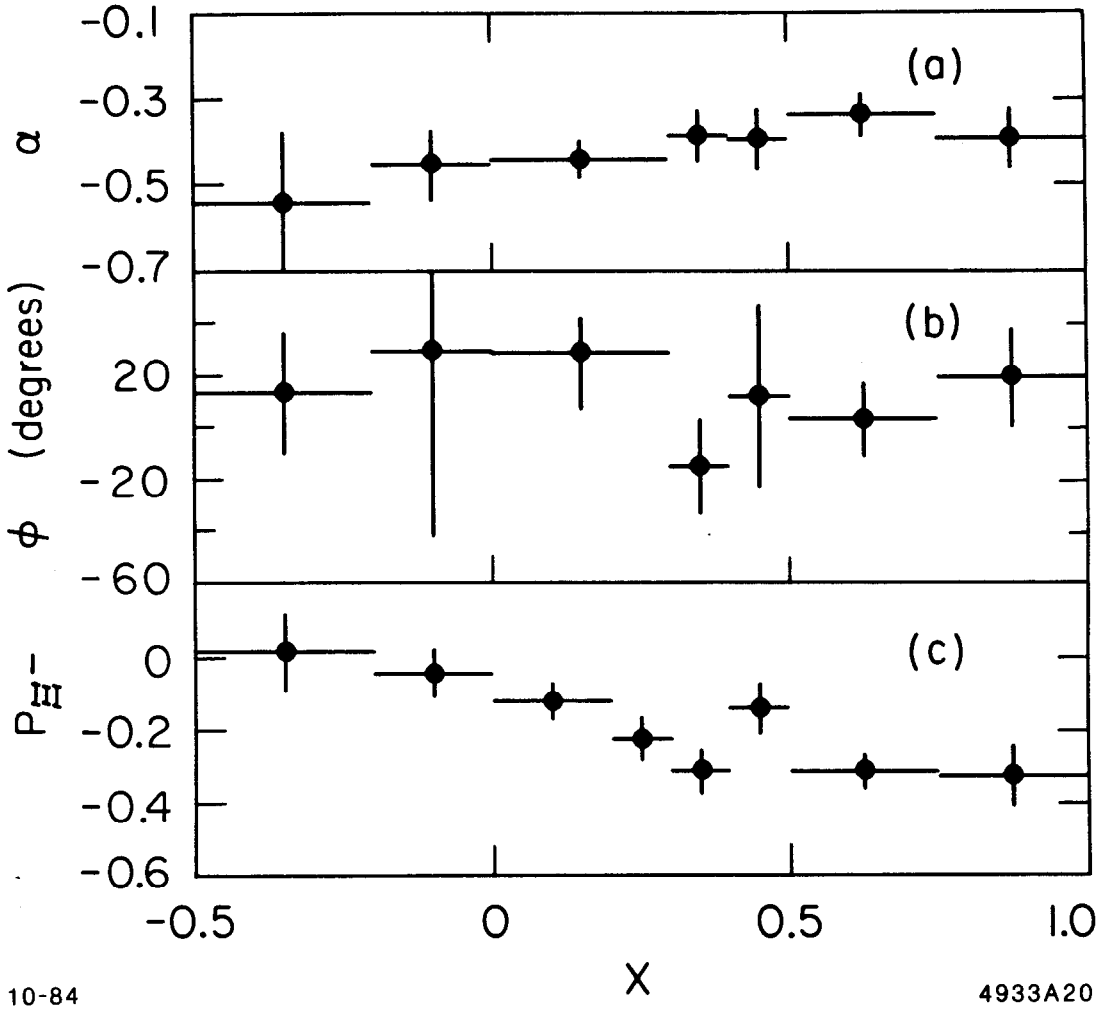
-0.1
-0.3
-0.5
-0.7
α
(a)
20
-20
-60
φ (degrees)
(b)
0
-0.2
-0.4
-0.6
P III
(c)
-0.5
0
0.5
1.0
X
10-84
4933A20

Fig. 19

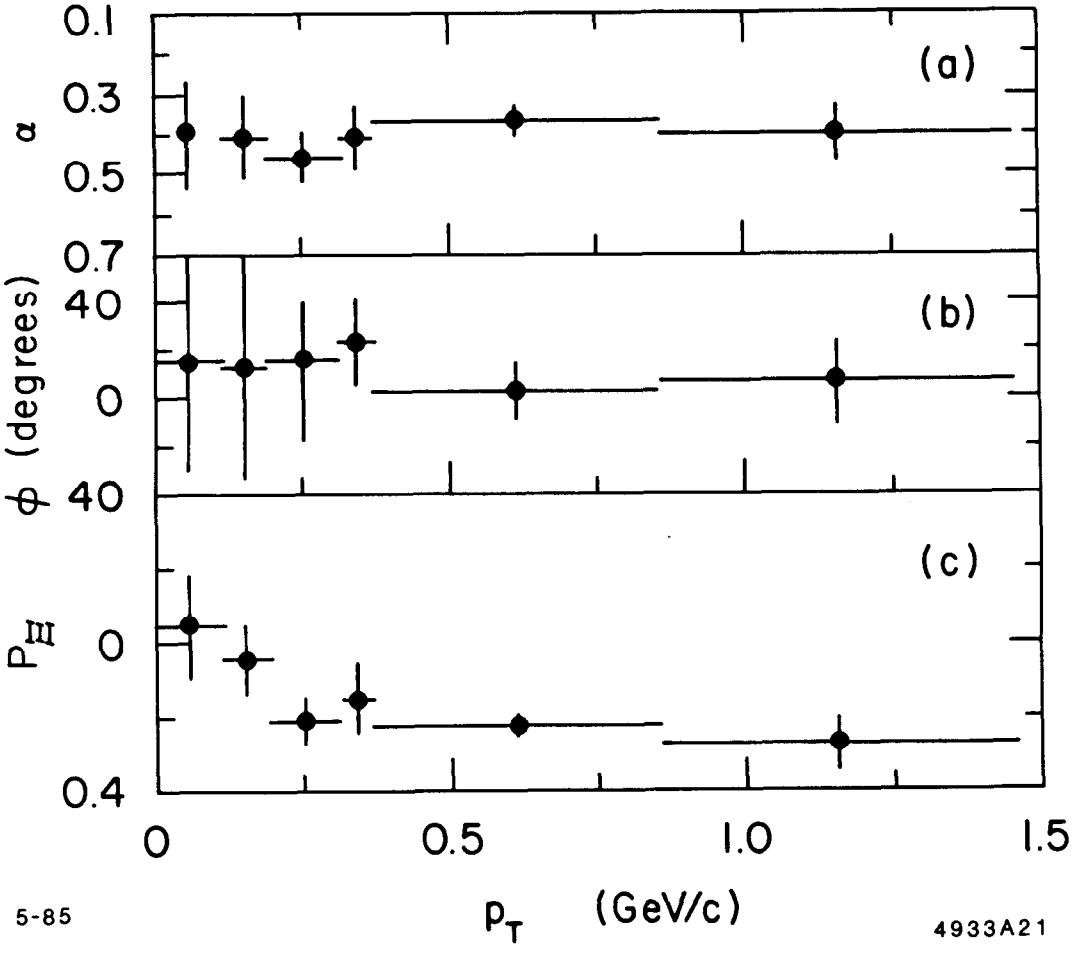
0.1
0.3
0.5
0.7
α
(a)
40
0
40
φ (degrees)
(b)
0
0.4
P_{III}
(c)
0
0.5
1.0
1.5
p_T (GeV/c)
5-85
4933A21

Fig. 20

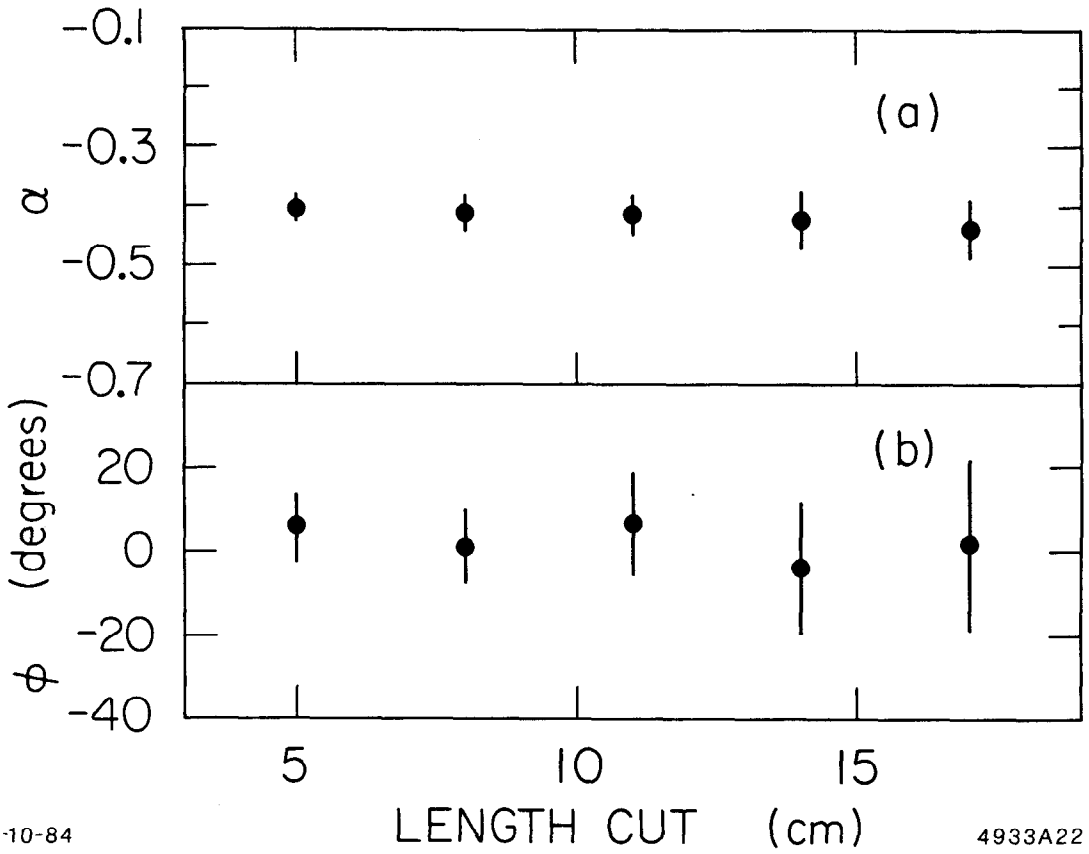
-0.1
-0.3
-0.5
-0.7
α
(a)
20
0
-20
-40
φ (degrees)
(b)
5
10
15
LENGTH CUT (cm)
10-84
4933A22

Fig. 21

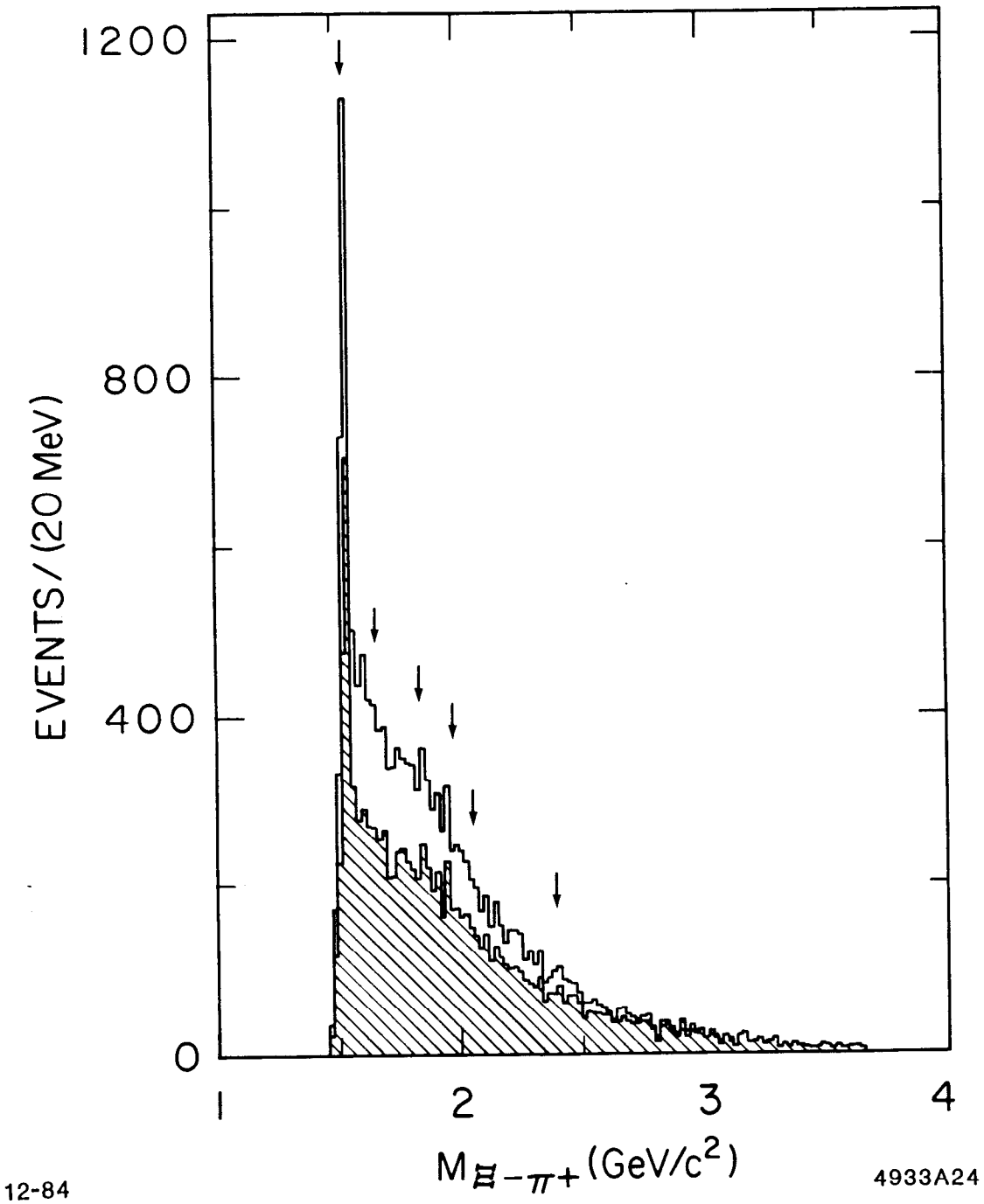

Fig. 22

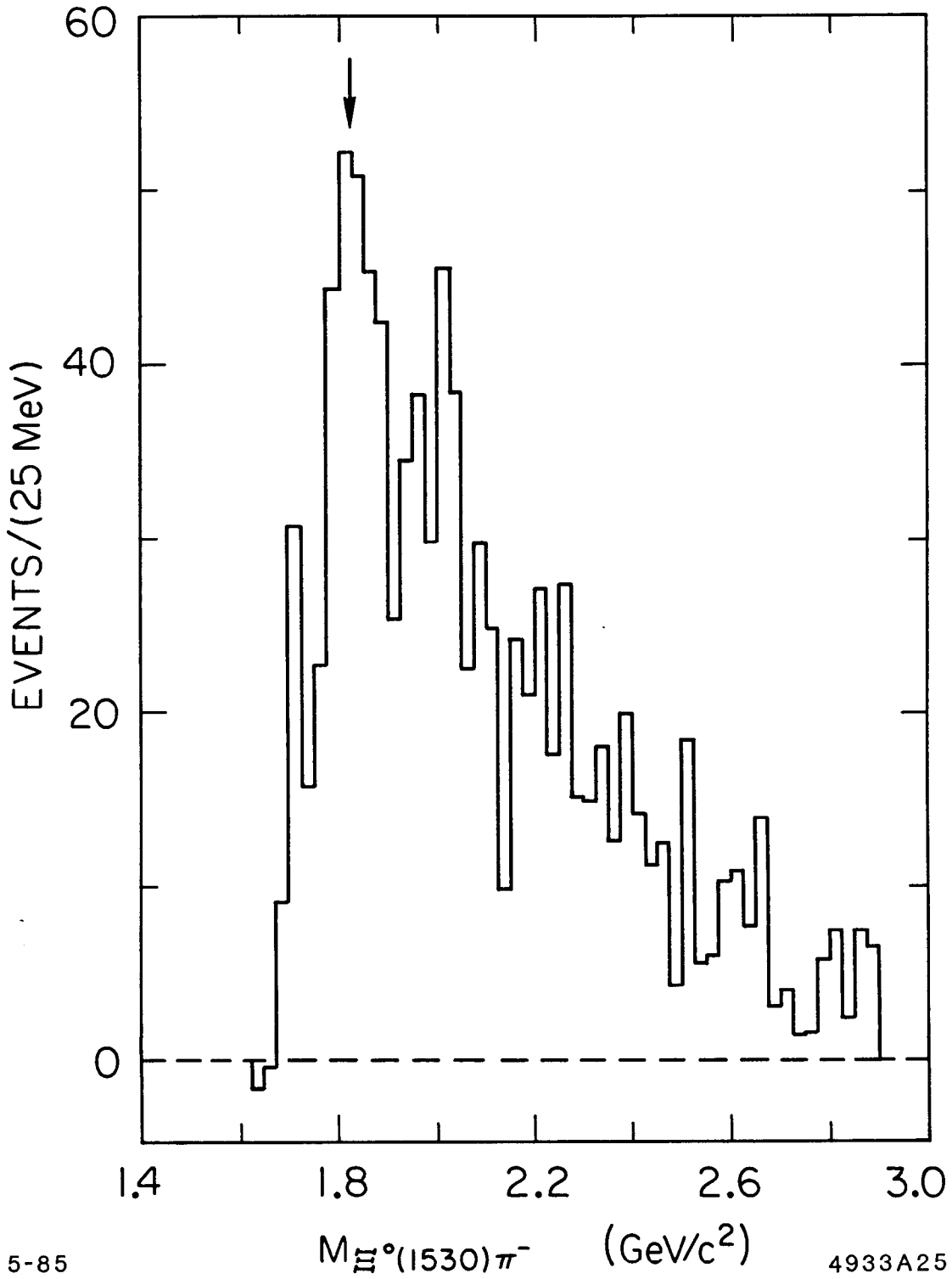
60
40
20
0
EVENTS/(25 MeV)
1.4
1.8
2.2
2.6
3.0
$M_{\Xi^0(1530)\pi^-}$ (GeV/c^2)
5-85
4933A25

Fig. 23

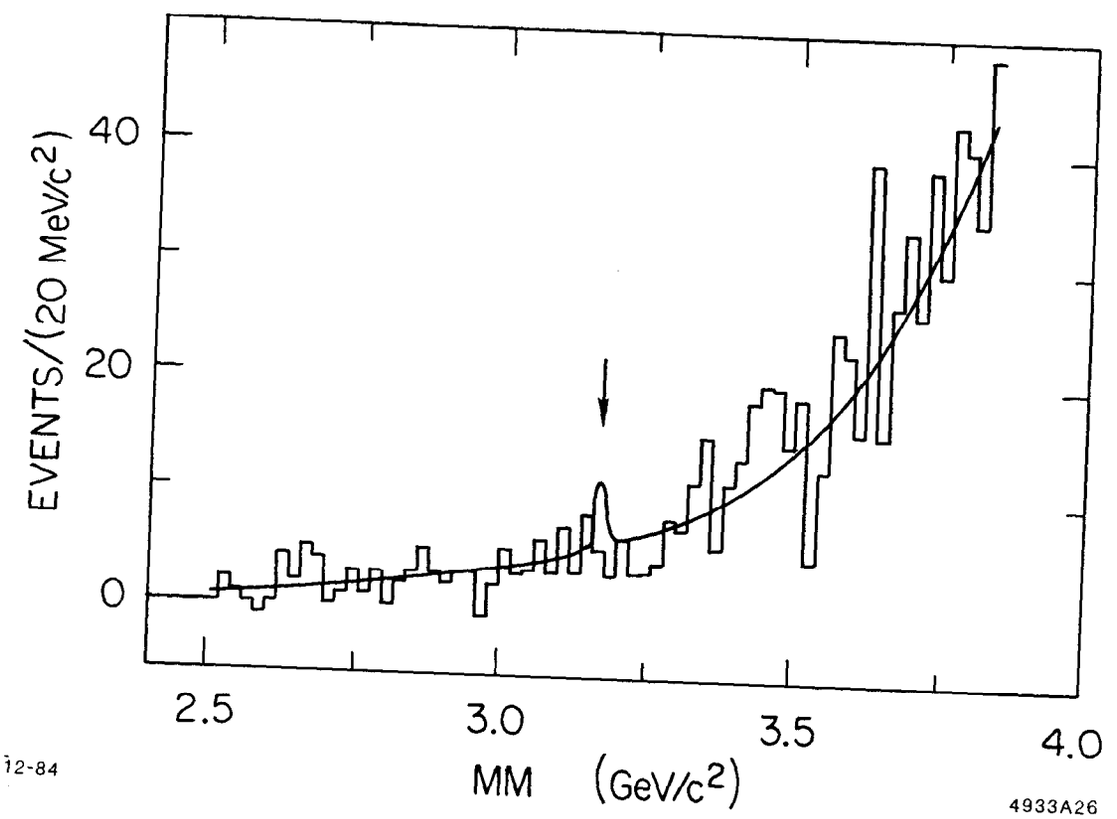

Fig. 24